Synchronization in Networks with Random Interactions: Theory and Applications

Jianfeng Feng[†] Viktor K. Jirsa[‡] Mingzhou Ding[*]

[†]Department of Computer Science and Mathematics

Warwick University, Coventry CV4 7AL, UK

[‡]Center for Complex Systems and Brain Sciences

Florida Atlantic University, Boca Raton, Florida 33431, USA

[*]Dept. of Biomedical Engineering. University of Florida

Gainesville, FL 32611, USA

November 22, 2005

Abstract

Synchronization is an emergent property in networks of interacting dynamical elements. Here we review some recent results on synchronization in randomly coupled networks. Asymptotical behavior of random matrices is summarized and its impact on the synchronization of network dynamics is presented. Robert May's results on the stability of equilibrium points in linear dynamics are first extended to nonlinear systems where the synchronized dynamics can be periodic or chaotic and then to systems with time delayed coupling. Finally, applications of our results to neuroscience, in particular, networks of Hodgkin-Huxley neurons, are included.

Behaviour and structures of interacting dynamical systems are complex. Most research on complex networks has been focused so far on networks with deterministic interactions. In this paper we study the behaviour of networks with random interactions. We extend Robert May's results on the stability of equilibrium points in linear dynamics to nonlinear systems where the synchronized dynamics can be periodic or chaotic and then to systems with time delayed coupling. Results are then applied to networks in Neuroscience.

1 Introduction

The developments in dynamical systems theory over the last few decades have provided the foundation for understanding the dynamics of networks of coupled dynamical systems [1, 2, 3, 4, 5, 6, 7, 8, 9, 10]. One central aim of the contemporary study of such networks is to understand how emergent activities of a network with nonlinear units arise from their (nonlinear) interactions [11, 12, 13, 14, 15, 16, 17, 18, 19, 20].

In the current review paper, we intend to answer this question for a specific emergent activity in a specific network topology: synchronization in a network with random interactions. Networks with random interactions have been intensively investigated and some well known models include (1) the spin glass model, which is a generalization of the Ising model , where the coupling strengths are simply independent identically distributed (i.i.d.) random variables [21]; and (2) the Hopfield model with correlated interactions derived from the Hebbian learning rule. The characterization of the properties of these models has been the central research topic of mathematical physics. It is worth noting that past research has primarily concentrated on the equilibrium properties of these models. One point of departure for our work is to investigate the full dynamical properties of such systems; a second point is to consider time delays in the random interactions.

One motivation of our research comes from biology, in particular, neuroscience. One might argue that in real biological situations, there are no networks with random interactions. Taking neuroscience as an example, one might argue that all networks are designed genetically or are modified according to certain learning rules such as the Hebbian learning rule. Hence we should pay attention to networks with specific and deterministic interactions. Is this viewpoint correct?

First, from a purely theoretical point of view, studying the properties of a network with random interactions has provided us with some fundamental revisions of our picture of network dynamics. Early in the 1970s, Robert May [22] showed that a simple network with random interactions is stable if and only if the network is not too large and the interactions are not too strong. A precise relation between the network size and the average interaction strength was derived. In recent years,

via the study of small-world networks and scale-free networks, we are able to apply our knowledge of randomly interacting networks to diverse areas of science and engineering. Most recently, IBM launched the Blue Brain project which is essentially based upon the notion of 'microcolumns': a network of neurons with random interactions.

Second, from a purely biological point of view, we know that the cortex is a enormously complex network and to completely unravel its mysteries is beyond the reaches of current technologies. This network is very dynamic in which the interactions change constantly, on the time scale of tens of milliseconds, and are dependent on the activity of participating neurons. If we take the viewpoint that neurons are stochastic units, then the connections (interactions) are necessarily random. To fully understand the dynamics of such a network, novel mathematical tools are required. It is our belief that the present theory on synchronized dynamics in networks with random interactions will partly serve the role.

Our current paper is centered around May's discussion [22] of the stability of linear networks with random interactions and we will extend these results along two lines, that is nonlinear network dynamics and random interactions with time delays. We first provide a brief review of May's 1972 result [22] in section 2. We then present a brief introduction to the theory of random matrices [23, 24] which will play a key role in our later developments. The mean maximal eigenvalue of a random matrix is calculated. Here the matrix elements could have independent, dependent or long-tailed distributions. In Section 3, we consider nonlinear dynamics with random interactions. Via some matrix transformation, the analysis of the stability of a synchronization state of a nonlinear system is reduced to finding the mean maximal eigenvalue of a dependent random matrix. Three cases are investigated in detail, corresponding to three distinct distributions for the interaction strengths. The results are obtained with the help of the extremal value theory in statistics and the Gershgorin disk theorem [25]. In Section 4, we discuss the stability of equilibrium solutions of networks with random delayed interactions [26]. Here we present completely analytical results for the cases of single discrete, as well as distributed time delays.

Finally, in Section 5, we turn our attention to the applications of our theory to neuroscience. The neuron model we employ in the current paper is the Hodgkin-Huxley model, a biophysical neuron model. Although the model is highly nonlinear, it has a smooth trajectory, in comparison with the simplest spiking neuron model: the integrate-and-fire model, which facilitates our analysis..

2 Background

2.1 Stability of linear systems with random interactions

Consider an N-dimensional state vector $\mathbf{x} = (\cdots x_i \cdots)$ with $x_i \in \mathcal{R}$ and $i = 1, \cdots, N$. Let the equations of motion in component form be

$$\dot{x}_i(t) = -x_i(t) + \sum_{j=1}^{N} b_{ij} x_j(t) \tag{1}$$

where $b_{ij} \in \mathcal{R}$ is the interaction or coupling strength. Letting $\mathbf{B} = (b_{ij})$ be the coupling matrix, (1) can be written as

$$\dot{\mathbf{x}}(t) = -\mathbf{x}(t) + \mathbf{x}(t)\mathbf{B}^T \tag{2}$$

where T stands for matrix transpose. Decompose the coupling matrix according to $\mathbf{B}^T = \mathbf{E}\Lambda\mathbf{E}^{-1}$ where Λ is the Jordan form with complex eigenvalues $\lambda \in \mathcal{C}$ and $\mathbf{E}$ contains the corresponding eigenvectors $\mathbf{e}$. Multiplying (2) from the right with $\mathbf{E}$ we obtain

$$d\mathbf{x}(t)\mathbf{E}/dt = -\mathbf{x}(t)\mathbf{E} + \mathbf{x}(t)\mathbf{E}\Lambda. \tag{3}$$

This leads to a decoupled representation of the dynamics of (2) in terms of its eigenmodes

$$\dot{\mathbf{u}}(t) = -\mathbf{u}(t) + \lambda\mathbf{u}(t), \quad \lambda \in \mathcal{C} \tag{4}$$

where $\mathbf{u} = \mathbf{x}\mathbf{e}$. Hence we reduced the discussion of the stability of the N-dimensional system in (1) to the study of the stability of the eigenmode which is a one dimensional system. Let the eigenvalue $\lambda = a + ib,\ a, b \in \mathcal{R}$. Clearly, for the eigenmode

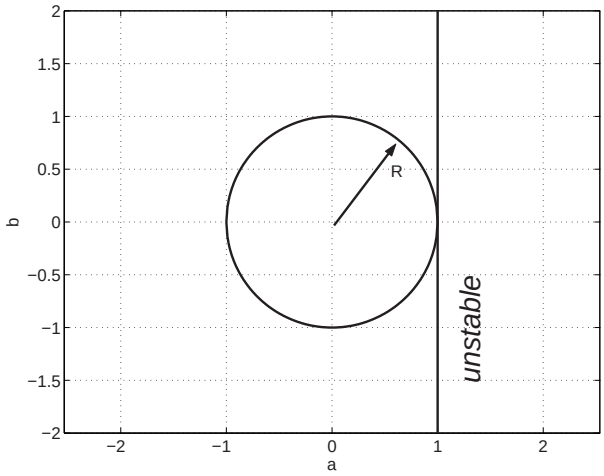

Figure 1: The stability region is constrained to the left half plane, $Re(\lambda) = a < 1$, within the complex λ plane as indicated by the vertical line. If all the eigenvalues of the coupling matrix $\mathbf{A}$ are contained in the unit disk, $R = 1$, then the system (2) is stable.

to be stable we must have $Re(\lambda) = a < 1$. The stability region in the complex λ plane is shown in Figure 1.

To study the stability of Eq. (2) as a function of system size N and coupling strength we follow the formulation of May[22]. Let

$$b_{ij} = \frac{ra_{ij}}{\sqrt{N}} \tag{5}$$

Here the variable r describes the connectivity of the coupled system. Specifically, we let $r = 1$ with probability C and $r = 0$ with probability $1 - C$. The variables a_{ij} are independent identically distributed Gaussian random variables with zero mean and standard deviation σ. Clearly, b_{ij} has zero mean and standard deviation $\sqrt{C}\sigma/\sqrt{N}$ which measures the average interaction strength between the elements in the system of size N. According to the theory of random matrices, for large N, the eigenvalues of the coupling matrix $\mathbf{B}$ are contained in the disk of radius $R = \sqrt{C}\sigma$ which is centered at the origin. If this disk is contained in the stability region shown in Figure 1 then the system is stable. Otherwise it is unstable. Combining this idea with the stability region plot in figure 1 we have

$$R = \sqrt{C}\sigma < 1 \tag{6}$$

as the stability condition which is the result obtained by May in 1972.

Hence the stability of (1) is completely determined by the maximal eigenvalue of a random matrix (see Section 2.3 for further discussions on this point). The theory of the maximal eigenvalue of a random matrix is an enormous field, covering areas as diverse as number theory and signal processing [27, 28, 29]. Here we review only very briefly some facts related to our results below.

2.2 Random matrix with short tail and independent distribution

Consider a symmetric $N \times N$ matrix $\mathbf{B}$, each element of which is an i.i.d (upper triangle, not including the diagonal) random variable with a finite second order moment. With some further minor restrictions, we have the following conclusion $''\lim''_{N\to\infty} \frac{\max(\mathrm{eig}(\mathbf{B}))}{\sqrt{N}} \to \xi$ where ξ is a constant and $''\lim''$ is understood in the sense of Eq. (7) below.

Similar to the law of large numbers, the maximal eigenvalue of a random matrix approaches a constant, after scaling with a factor $1/\sqrt{N}$. To numerically test the results, in Fig. 2 upper left panel we plot the scaled mean maximal eigenvalue of the matrix $\mathbf{B} = (\mathbf{A} + \mathbf{A}^T)/\sqrt{N}$ vs. N, where the elements of the matrix A are i.i.d normally distributed random variables with mean 0 and variance 1. The middle line in the figure is the mean and the other two lines are the mean $\pm$ standard deviation. As N increases, the mean maximal eigenvalue of the random matrix $(\mathbf{A} + \mathbf{A}^T)/\sqrt{N}$ increases first and stabilizes rapidly. More precisely we have

$$\max(\mathrm{eig}(\mathbf{B})) \sim 1.983\sqrt{N}$$

The upper right panel in Fig. 2 is the mean maximal eigenvalue of the matrix $\mathbf{B} = \mathbf{A}$ vs. N. It is easily seen that now $\xi = 1$.

In Fig. 2 bottom left panel, the mean maximal eigenvalues of an i.i.d symmetric matrix vs. standard deviation of diagonal elements are depicted (dotted lines). In comparison, the solid lines are the mean maximal eigenvalues of the identity matrix but with a deterministic diagonal equal to the standard deviation. It is interesting

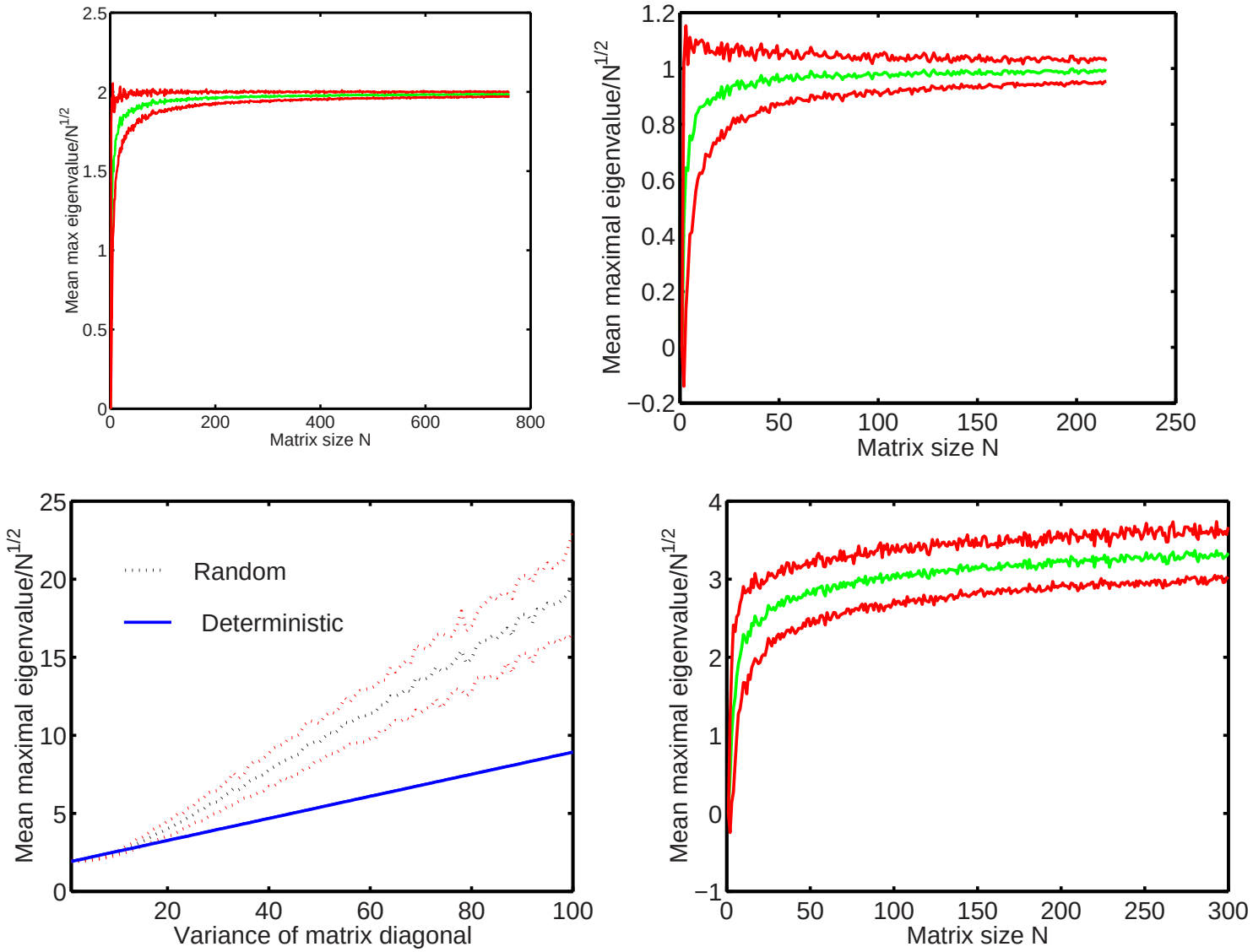

Figure 2: Upper panel left, mean maximal eigenvalue (middle line) and mean maximal eigenvalue $\pm$ standard deviation of maximal eigenvalue of the matrix $(\mathbf{A} + \mathbf{A}^T)/\sqrt{N}$ vs. matrix size N. Upper panel right, mean maximal eigenvalue (middle line) and mean maximal eigenvalue $\pm$ standard deviation of maximal eigenvalue of the matrix $\mathbf{B} = \mathbf{A}$ vs. matrix size N. Bottom panel left, mean maximal eigenvalue vs. standard deviation of the diagonal elements (dotted lines) and mean maximal eigenvalue $\pm$ standard deviation of maximal eigenvalue. Solid lines is mean maximal eigenvalue vs. the actual value of the diagonal elements (not random) and mean maximal eigenvalue $\pm$ standard deviation of maximal eigenvalue. Bottom panel right, mean maximal eigenvalue vs. matrix size N with $\mathbf{B} = \mathbf{A}$ and $b_{ii} = -\sum_{j \neq i} b_{ij}$.

to see that in this case the maximal eigenvalues are more deterministic: the standard deviation is very small so that the three lines nearly coincide with one another. In Fig. 2 bottom panel right, the mean maximal eigenvalue of a symmetric matrix with $b_{ii} = -\sum_{j \neq i} b_{ij}$ is shown. The matrix of this type will be used frequently in the next sections. Comparing Fig. 2 top right with bottom right, it is interesting to see that the condition $b_{ii} = -\sum_{j \neq i} b_{ij}$ ensures the mean maximal eigenvalues being larger (around 2.8).

For a symmetric matrix with i.i.d random variables with mean zero and variance σ, we have the following Tracy-Widom law:

$$\lim_{N \to \infty} P((\max(\text{eig}(B)) - 2\sigma\sqrt{N}) \leq s) = F(s\sigma/N^{1/6}) \tag{7}$$

where

$$F(s) = \exp\left(-\frac{1}{2}\int_s^\infty q(x)dx - \frac{1}{2}\int_s^\infty (x-s)q^2(x)dx\right)$$

and $q(x)$ is the unique solution (Hastings-McLeod solution) of the Painleve II equation

$$q'' = sq + 2q^3$$

In other words, the maximal eigenvalue of the random matrix B is around $2\sigma\sqrt{N}$ where the fluctuation around this value is on the order of $N^{1/6}$.

2.3 Random matrix with long tail or dependent distributions

In the previous subsection, we have looked at the behavior of the maximal eigenvalue of a Wigner's matrix: the elements of the matrix have a finite second order moment and are independent. In recent years, however, there are research efforts devoted to random matrices with long-tail distributions or dependent elements. Examples include small-world networks and scale-free networks [5]. The asymptotic behavior of the maximal eigenvalue of such matrices could be dramatically different from the behavior considered in the previous subsection.

In Fig. 3 left, the mean maximal eigenvalue of a random matrix **B** with each element having a distribution density (Pareto distribution)

$$2/x^3, x \geq 1$$

is plotted. It is clearly shown that its asymptotic activity is proportional to N rather than $\sqrt{N}$. In other words we have

$$\frac{\max(\text{eig}(B))}{N} \to \xi$$

where ξ is a constant. This phenomenon reminds us of the definition of stable distributions in classical probability theory (see for example page 170 in [30]). A distribution of an i.i.d sequence y_i is stable if for each N there exist constants $c_N > 0, \gamma_N$ such that

$$\sum_i y_i = c_N y_1 + \gamma_N$$

where $=$ is understood in the sense of distribution. When $c_N = N^{1/\alpha}$, α is called the characteristic exponent of y_i. It is clear that the normalization factor before the mean maximal eigenvalue is related to c_N, or the characteristic exponent. To the best of our knowledge, an analytical proof of the fact is lacking.

In Fig. 3 right, the dependence of the mean maximal eigenvalue of a random matrix **B** on the matrix size as well as the correlation coefficient between elements is shown. The larger the correlation coefficient, the smaller the mean maximal eigenvalue of a random matrix. Hence according to May's argument, positively correlated random interactions make a system more stable than i.i.d. interactions.

2.4 A Theoretical remark

May's results are simple but interesting and have attracted a lot of attention in the literature [31, 32, 33, 34, 35, 36, 37, 38, 39, 40, 41, 42, 43]. In particular, in 1984, Cohen and Newman [32, 44] were able to present counter examples to show that May's conclusions did not hold true for some cases, although they were not able to establish a correct one. Hence whether May's criteria are true or not for a given distribution remains an open problem, after more than 30 years of research.

Recently, in mathematical physics, researchers have developed many techniques to tackle systems with random interactions. Two of the most known examples are the spin glass model and the Hopfield model. With the help of some techniques developed there, we have been able to establish a theory for a linear system with random interactions, which proves and extends May's results.

We need some further (minor) restrictions on the matrix B. Assume there exists $\alpha > 0$ such that

$$P\{|ra_{ij}| > \lambda\} \leq C_1 e^{-C_1 \lambda^\alpha}, \quad (\forall \lambda > 0) \tag{8}$$

Supply the system with the initial conditions:

$$\mathbf{x(0)} = \mathbf{c}, \quad \mathbf{c} = (\mathbf{1}, \ldots, \mathbf{1}) \in \mathbf{R^N} \tag{9}$$

We are interested in the statistical distribution of $\{x_i(t)\}_{i=1}^N$ on the real line. To study this distribution for any fixed time t we define a normalized counting function of x_i.

$$\mathcal{N}_N(\lambda, t) = N^{-1} \sharp\{x_i(t) \leq \lambda\} = N^{-1} \sum_{i=1}^{N} \theta(\lambda - x_i(t)), \tag{10}$$

where $\theta(x)$ is a standard Heaviside function. This function is a distribution of the random discrete measure on the real line. Our goal is to study the behavior of this measure in the limit $N \to \infty$. More precisely, we prove that this measure becomes non random, as $N \to \infty$ (i.e. the variance of $\mathcal{N}_N(\lambda, t)$ tends to zero) and the mean value coincides with the function

$$\lim_{N \to \infty} E\{\mathcal{N}_N(\lambda, t)\} = \int_{-\infty}^{\lambda} dx \frac{e^{-(x-a(t))^2/2\sigma(t)}}{\sqrt{2\pi\sigma(t)}}. \tag{11}$$

This means that $\mathcal{N}_N(\lambda, t)$ becomes a normal distribution with a mean value $a(t)$ and the variance $\sigma(t)$ defined below.

Theorem 1 *(Feng, Shcherbina, and Tirozzi[45]) Consider the system (1) with a matrix B of the form (5) with mean zero and variance $\sqrt{C}\sigma$, under the condition (8). Supply this system with the initial conditions (9). Then for any $t > 0$, $\mathcal{N}_N(\lambda, t)$ defined by (10) converges in probability to the normal distribution $N(a(t), \sigma(t))$ (11) with the mean value*

$$a(t) = e^{-t} \tag{12}$$

and the variance

$$\sigma(t) = e^{-2t} \sum_{m=1}^{\infty} \frac{(\sqrt{C}\sigma t)^{2m}}{m!m!}. \tag{13}$$

In other words, the system is stable if and only if $\lim_{t\to\infty} \sigma(t) < \infty$. This is equivalently to saying that $\sqrt{C}\sigma \leq 1$ is the necessary and sufficient condition for the dynamics in (1) to be stable. The theorem above can be extended to the case with general initial conditions.

3 Synchronization in randomly coupled nonlinear systems

In this section, we consider the synchronization problem for a network of interacting nonlinear dynamical systems, extending the results above for equilibrium solutions to more general dynamical behavior. We show that, essentially, the problem can be reduced to analyzing the maximal eigenvalue of a correlated random matrix, as discussed in the previous section[46, 47, 48].

Since the coupling matrix is correlated, we are not able to obtain a sufficient and necessary condition as in the previous and the next section. However, with the help of the extremal value theory in statistics and the Gershgorin disc theorem, a sufficient condition for the stability of a synchronized state, chaotic or periodic, to be stable is obtained.

3.1 Preliminary results

3.1.1 Coupled Maps

The system we consider is represented by

$$\mathbf{x}^i(t+1) = \mathbf{f}(\mathbf{x}^i(t)) + \frac{1}{N} \sum_{j=1}^{N} b_{ij} \cdot \mathbf{H}(\mathbf{x}^j(t)), \tag{14}$$

where $\mathbf{x}^i(t)$ is the M-dimensional state vector of the ith map at time t and $\mathbf{H} : R^M \to R^M$ is the coupling function [49]. We define $\mathbf{B} = [b_{ij}]$ as the coupling

matrix where b_{ij} gives the stochastic interaction strength from map j to map i. The condition $\sum_j b_{ij} = 0$ is imposed to ensure that synchronized dynamics is a solution to Eq. (14) (see previous section). Note that the coupling matrix is scaled differently from that in Section 2.

Linearizing Eq.(14) around the synchronized state $\mathbf{x}(t)$, which evolves according to $\mathbf{x}(t+1) = \mathbf{f}(\mathbf{x}(t))$, we have

$$\mathbf{z}^i(t+1) = \mathbf{J}(\mathbf{x}(t)) \cdot \mathbf{z}^i(t) + \frac{1}{N} \sum_{j=1}^{N} b_{ij} \cdot D\mathbf{H}(\mathbf{x}(t)) \cdot \mathbf{z}^j(t), \tag{15}$$

where $\mathbf{z}^i(t)$ denotes the ith map's deviations from $\mathbf{x}(t)$, $\mathbf{J}(\cdot)$ is the $M \times M$ Jacobian matrix for $\mathbf{f}$ and $D\mathbf{H}(\cdot)$ is the Jacobian of the coupling function $\mathbf{H}$. In terms of the $M \times N$ matrix $\mathbf{S}(t) = (\mathbf{z}^1(t)\ \mathbf{z}^2(t)\ \cdots\ \mathbf{z}^N(t))$, Eq. (15) can be recast as

$$\mathbf{S}(t+1) = \mathbf{J}(\mathbf{x}(t)) \cdot \mathbf{S}(t) + \frac{1}{N} D\mathbf{H}(\mathbf{x}(t)) \cdot \mathbf{S}(t) \cdot \mathbf{B}^T. \tag{16}$$

According to the theory of Jordan canonical forms, the stability of Eq. (16) is determined by the eigenvalue λ of $\mathbf{B}$. Denote the corresponding eigenvector by $\mathbf{e}$ and let $\mathbf{u}(t) = \mathbf{S}(t)\mathbf{e}$. Then

$$\mathbf{u}(t+1) = (\mathbf{J}(\mathbf{x}(t)) + \frac{1}{N} \lambda \cdot D\mathbf{H}(\mathbf{x}(t))) \cdot \mathbf{u}(t). \tag{17}$$

So the stability problem originally formulated in the $M \times N$ space has been reduced to a problem in a $M \times M$ space where it is often the case that $M \ll N$.

We note that $\lambda = 0$ is always an eigenvalue of $\mathbf{B}$ and its corresponding eigenvector is $(1\ 1\ \cdots\ 1)^T$ due to the synchronization constraint $\sum_{j=1}^{N} b_{ij} = 0$. In this case, Eq. (17) can be used to generate the Lyapunov exponents for the individual system[50], which we denote by $h_1 = h_{max} \geq h_2 \geq \cdots \geq h_M$. These exponents describe the dynamics within the synchronization manifold defined by $\mathbf{x}^i = \mathbf{x}\ \forall i$.

The subspace spanned by the remaining eigenvectors is transverse to the synchronization manifold, which will be stable if the transverse Lyapunov exponents are all negative[51, 52]. To examine this problem, we treat λ in Eq. (17) as a complex parameter and calculate the maximum Lyapunov exponent μ_{max} as a function of λ. This function is referred to as the master stability function by Pecora and

Carroll[10]. The region in the $(\mathrm{Re}(\lambda), \mathrm{Im}(\lambda))$ plane, where $\mu_{max} < 0$, defines a stability zone denoted by Ω. There are two possible configurations of Ω. Whether Ω is an unbounded area or a bounded one is contingent on the coupling scheme and other system parameters. The origin, which is the zero eigenvalue of $\mathbf{B}$, may or may not lie in the stability zone. For example, for equilibrium or periodic state in coupled maps, the origin is in Ω, but for chaos, it lies outside of Ω. We note that, typically, Ω is obtained numerically. In some instances analytical results are possible (see below).

Clearly, if all the transverse eigenvalues of $\mathbf{B}$ lie within Ω, then the synchronized state is stable. Here we seek constraints applicable directly to the coupling strengths. This problem is dealt with by combining the master stability function with the Gershgorin disc theory.

Gershgorin disc theorem: The Gershgorin disc theorem [53] states that all the eigenvalues of a $n \times n$ matrix $\mathbf{A} = [a_{ij}]$ are located in the union of n discs (called Gershgorin discs) where each disc is given by

$$\{z \in C : |z - a_{ii}| < \sum_{j \neq i} |a_{ji}|\}, \quad i = 1, 2, \ldots, n. \tag{18}$$

To apply this theorem to the transverse eigenvalues we need to remove $\lambda = 0$. We appeal to an order reduction technique in matrix theory[25] which leads to a $(T-1) \times (T-1)$ matrix $\mathbf{D}$ whose eigenvalues are the same as the eigenvalues of $\mathbf{B}$ except for $\lambda = 0$.

Suppose that, for a given matrix $\mathbf{B}$, we have knowledge of one of its eigenvalues $\tilde{\lambda}$ and the eigenvector $\mathbf{e}$. Through proper normalization we can make any component of $\mathbf{e}$ equal one. Here, without loss of generality, we assume that the first component is made equal 1, namely, $\mathbf{e} = (1, \mathbf{e}_{N-1}^T)^T$. Rewrite $\mathbf{B}$ in the following block form:

$$\mathbf{B} = \begin{pmatrix} b_{11} & \mathbf{r}^T \\ \mathbf{s} & \mathbf{B}_{N-1} \end{pmatrix} \tag{19}$$

with $\mathbf{r} = (b_{12}, \cdots, b_{1N})^T$, $\mathbf{s} = (b_{21}, \cdots, b_{N1})^T$ and

$$\mathbf{B}_{N-1} = \begin{pmatrix} b_{22} & \cdots & b_{2N} \\ \vdots & \vdots & \vdots \\ b_{N2} & \cdots & b_{NN} \end{pmatrix}. \tag{20}$$

Choose a matrix $\mathbf{P}$ in the form

$$\mathbf{P} = \begin{pmatrix} 1 & \mathbf{0}^T \\ \mathbf{e}_{N-1} & \mathbf{I}_{N-1} \end{pmatrix}. \tag{21}$$

Here $\mathbf{I}_{N-1}$ is the $(T-1) \times (T-1)$ identity matrix. Similarity transformation of $\mathbf{B}$ by $\mathbf{P}$ yields

$$\mathbf{P}^{-1}GP = \begin{pmatrix} \tilde{\lambda} & \mathbf{r}^T \\ \mathbf{0} & \mathbf{B}_{N-1} - \mathbf{e}_{N-1}\mathbf{r}^T \end{pmatrix}. \tag{22}$$

Since $\mathbf{P}^{-1}BP$ and $\mathbf{B}$ have identical eigenvalue spectra, the $(T-1) \times (T-1)$ matrix

$$\mathbf{D}^1 = \mathbf{B}_{N-1} - \mathbf{e}_{N-1}\mathbf{r}^T \tag{23}$$

assumes the eigenvalues of $\mathbf{B}$ excluding $\tilde{\lambda}$. We can obtain N different versions of the reduced matrix, which we denote by $\mathbf{D}^k$ $(k = 1, 2, \cdots, N)$, depending on which component of $\mathbf{e}$ is made equal 1.

Applying the above technique to the coupling matrix B by letting $\tilde{\lambda} = 0$ and $\mathbf{e} = (1\ 1\ \cdots\ 1)^T$ we get $\mathbf{D}^k = [d_{ij}^k]$ where $d_{ij}^k = b_{ij} - b_{kj}$. From the Gershgorin theorem the stability conditions of the synchronized dynamics are expressed as

1. The center of every Gershgorin disc of $\mathbf{D}^k$ lies inside the stability zone Ω. That is, $(b_{ii} - b_{ki}, 0) \in \Omega$.

2. The radius of every Gershgorin disc of $\mathbf{D}^k$ satisfies the inequality

$$\sum_{j=1, j\neq i}^{N} \frac{|b_{ji} - b_{ki}|}{N} < \delta(\frac{b_{ii} - b_{ki}}{N}), \quad i = 1, 2, \ldots, N \quad \text{and} \quad i \neq k. \tag{24}$$

   Here $\delta(x)$ is the distance from point x on the real axis to the boundary of the stability zone Ω.

3. As k varies from 1 to N, we obtain N sets of stability conditions of Eq. (24). Each one provides sufficient conditions constraining the coupling strengths.

3.1.2 Coupled ODE's

The above procedure for obtaining stability bounds can also be applied to coupled identical ODEs written as

$$\dot{\mathbf{x}}^i = \mathbf{F}(\mathbf{x}^i) + \frac{1}{N}\sum_{j=1}^{N} b_{ij}\mathbf{H}(\mathbf{x}^j), \tag{25}$$

where $\mathbf{x}^i$ is the M-dimensional vector of the ith node and the dot denotes time derivative. The dynamics of the individual node is $\dot{\mathbf{x}} = \mathbf{F}(\mathbf{x})$. Linearizing around the synchronized state we get

$$\dot{\mathbf{z}}^i = \mathbf{J}(\mathbf{x}) \cdot \mathbf{z}^i + \frac{1}{N}\sum_{j=1}^{N} b_{ij} \cdot D\mathbf{H}(\mathbf{x}) \cdot \mathbf{z}^j, \tag{26}$$

where $\mathbf{z}^i$ denotes deviations from $\mathbf{x}$, $\mathbf{J}(\cdot)$ and $D\mathbf{H}(\cdot)$ are the $M \times M$ Jacobian matrices for the functions of $\mathbf{F}$ and $\mathbf{H}$. Adopting Jordan canonical form, we obtain

$$\dot{\mathbf{u}} = \left[\mathbf{J}(\mathbf{x}) + \frac{1}{N}\lambda \cdot D\mathbf{H}(\mathbf{x})\right]\mathbf{u}, \tag{27}$$

where λ is an eigenvalue of $\mathbf{B}$. Performing the same analysis as for coupled maps, we obtain the same stability conditions as given above.

3.2 Results

Now we turn to the stochastic case. Due to the synchronization constraint $\sum_{j=1}^{N} b_{ij} = 0$, the method based on i.i.d. random matrices is no longer applicable here, and we derive bounds on the random interactions using the criteria given in the previous subsection.

We see that the following inequality

$$\frac{\sum_{j=1,j\neq i}^{N} |b_{ji} - b_{ki}|}{N} - \delta\left(\frac{b_{ii}}{N} - \frac{b_{ki}}{N}\right) < 0 \tag{28}$$

implies Eq. (24). For simplicity of notation we further assume that $b_{ij}, i \neq j$ are i.i.d random array. Hence

$$\frac{\sum_{j=1,j\neq i}^{N} |b_{ji} - b_{ki}|}{N} \to \langle |b_{ji} - b_{ki}||b_{ki}\rangle \tag{29}$$

as N is large, where $\langle\cdot|\cdot\rangle$ is the conditional expectation. As a consequence of Eq. (29) and Eq. (24), we conclude that

$$\min_k \left[\max_i \left(\langle |b_{ji} - b_{ki}||b_{ki}\rangle - \delta\left(-\langle b_{12}\rangle - \frac{b_{ki}}{N}\right)\right)\right] < 0 \tag{30}$$

is a sufficient condition to ensure that the synchronized state is stable. Assume that the distribution density of G_{ij} is $p(x)$, we have

$$\langle |b_{ji} - b_{ki}||b_{ki}\rangle = \int |x - b_{ki}|p(x)dx.$$

Note that $\langle |b_{ji} - b_{ki}||b_{ki}\rangle$ could be infinity. After omitting the higher order term $\frac{b_{ki}}{N}$, we see that Eq. (86) is equivalent to requiring

$$\min_k \left[\max_i \langle |b_{ji} - b_{ki}||b_{ki}\rangle\right] < \delta\left(-\langle b_{12}\rangle\right).$$

The left hand side of the inequality above is independent of j and the right hand side of it is independent of k, i. Next we consider the behavior of

$$\eta_{ki} = \langle |b_{ji} - b_{ki}||b_{ki}\rangle.$$

There are three different behaviors, corresponding to three types of distribution in the extremal value theory.

1. **Global-stable**. This corresponds to the case of Type III of the extreme value theory[54]. In this case, we assume that $p(x)$ has a compact support set, i.e. b_{ij} is bounded. Hence $\min_k \max_i \eta_{ki}$ is again a bounded variable. The synchronization state is stable if

   $$\min_k \max_i \eta_{ki} < \delta\left(-\langle b_{12}\rangle\right),$$

   and the stability is independent of the system size N.

2. **Exponential-stable**. This case is the Type I distribution of the extreme value theory. For example, if we assume that $b_{ki}, k \neq i$ is exponentially distributed, we then have

   $$\max_i \eta_{ki} \sim \log N$$

   Therefore the Gershgorin disc increases at an order of $\log N$. The system is stable under the condition that

   $$N < C \exp\left(\delta(-\langle b_{12}\rangle)\right) \tag{31}$$

   where C is a positive constant.

3. **Power-stable**. This case is the Type II distribution of the extreme value theory. For example, if we assume that η_{ki} is distributed according to the Pareto distribution (long-tail distribution), i.e. the distribution density is $\alpha K x^{-\alpha-1},\ x \geq K^{1/\alpha}, \alpha > 0, K > 0$, we then have

$$\max_i \eta_{ki} \sim N^{1/\alpha}$$

provided that η_{ki} is finite almost surely. Hence the system is stable if

$$N < (\delta(-\langle b_{12} \rangle))^{\alpha} \cdot C$$

where C is a positive constant.

The physical meaning of the three-type behaviors is very clear. For the global-stable case, since the variation between interactions b_{ij} is small (bounded), we could expect that the synchronization state could be stable, independent of the system size N. For the exponential-stable and power-stable case, the synchronization state is stable when the system is finite. Essentially, Type I distribution indicates that the random interaction is exponentially distributed. The variance between interactions is greater than the bounded interaction case, but it is smaller than the power-stable case which corresponds to a long-tail distribution.

Finally we want to point out that the conditions developed in this section are sufficient. For the concrete examples in the next section where we can exactly calculate the stable region of the synchronization state, our conclusions below are sufficient and necessary. For a system with global-stable interactions, the system size can increase and the synchronization state is always stable. For exponential-stable and power-stable interactions, the system size can not increase without limit before the synchronization state loses its stability. For exponential-stable interactions, the size N can be greater than that with power-stable interactions.

3.3 Examples

We now illustrate the general approach by applying the above results to two examples where analytical results are possible. In the first example we consider

the coupled differential equation systems with $\mathbf{H}(\mathbf{x}) = \mathbf{x}$[47]. It is easy to see that $D\mathbf{H}$ is a $M \times M$ identity matrix. The Lyapunov exponents for Eq. (27) are easily calculated since the identity matrix commutes with $\mathbf{J}(\mathbf{x})$. Denoting them by $\mu_1(\lambda)$, $\mu_2(\lambda)$, ..., $\mu_M(\lambda)$, we have

$$\mu_i(\lambda) = h_i + \frac{1}{N}\mathrm{Re}(\lambda), \quad i = 1, 2, \ldots, M. \tag{32}$$

For stability, we require the transverse Lyapunov exponents ($\lambda \neq 0$) to be negative. This is equivalent to the statement that the maximum Lyapunov exponent is less than zero:

$$\mu_{max}(\lambda) = h_{max} + \frac{1}{N}\mathrm{Re}(\lambda) < 0. \tag{33}$$

In other words, the stability zone Ω is the region defined by $\mathrm{Re}(\lambda) < -Nh_{max}$. The distance function from the center of each Gershgorin disc to the stability boundary is given by: $\delta(b_{ii} - b_{ki}) = -h_{max} - (b_{ii} - b_{ki})$ $(i = 1, \ldots, N, \quad i \neq k)$. Thus the k-th set of stability conditions are

$$(b_{ii} - b_{ki}) < -Nh_{max}, \tag{34}$$

$$\sum_{j=1, j\neq i}^{N} |b_{ji} - b_{ki}| < -Nh_{max} - (b_{ii} - b_{ki}), \tag{35}$$

$$i = 1, 2, \ldots, N, \quad i \neq k.$$

It is obvious that the second inequality implies the first one. So the stability condition for the synchronized state (whether an equilibrium, periodic or chaotic state) is given by

$$\sum_{j=1, j\neq i}^{N} |b_{ji} - b_{ki}| + (b_{ii} - b_{ki}) < -Nh_{max}, \quad i = 1, 2, \ldots, N, \quad i \neq k. \tag{36}$$

When the interaction is i.i.d., we see that

$$\min_k \max_i \langle |b_{ji} - b_{ki}| | b_{ki} \rangle < -h_{\max} + (\langle b_{12} \rangle)$$

is a sufficient condition to ensure the stability of the synchronization state.

When the coupling is symmetric, i.e. $b_{ij} = b_{ji}$, Rangarajan and Ding [55], based on the use of Hermitian and positive semidefinite matrices, derived a very simple stability constraint

$$b_{ij} > h_{max}, \quad \forall\ i, j. \tag{37}$$

We assume that $(N-1)(N-2)/2$ random variables $b_{ij}, i = 1, 2, N-1, j > i$ are i.i.d. . Then Eq. (37) is reduced to

$$\min_{i<j} b_{ij} > h_{\max}$$

or equivalently

$$\max_{i<j}(-b_{ij}) < -h_{\max}.$$

Hence we have three different behaviors, as described before.

1. **Global-stable**. For example, $-b_{i,j}, i < j$ are uniformly distributed in $[0, -h_{\max}]$.

2. **Exponential-stable**. For example, $-b_{ij}, i < j$ are normally distributed with mean 0 and variance 1. We then know that

$$\max_{i<j}(-b_{ij}) = \max_{i<j} b_{ij} \tag{38}$$

and

$$\langle \max_{i<j} b_{ij} \rangle = b_N + \left[\int x \exp \exp(-\exp(-x)) \exp(-x) dx \right] / a_N$$

where

$$\begin{cases} a_N &= \sqrt{\log[(N-1)(N-2)/2]} \\ b_N &= a_N - 1/2\{\log\ \log[(N-1)(N-2)/2] + \log 4\pi\}/a_N. \end{cases}$$

Now we are in the position to compare our results with results in the literature. In [22], under similar setup (without the requirement of the symmetry of the matrix) with a linear dynamics, it is pointed out that if and only if $\sqrt{N} < 1$ the dynamics is stable, and it is unstable otherwise. It is readily seen that $b_N \sim a_N$ when N is large. Hence Eq. (38) is

$$(N-1)(N-2) < 2\exp(-h_{max})$$

In other words when $\sqrt{N} <$ constant, the dynamics is stable. As we pointed out before, when Eq. (38) is a necessary and sufficient condition (in the linear dynamics case, it is true), we can further assert that when

$$(N-1)(N-2) > 2\exp(-h_{max})$$

the dynamics is not stable.

3. **Power-stable**. From the extreme value theory we conclude that

$$\langle \max\{-b_{ij}\}\rangle / \sqrt{(N-1)(N-2)/2} = \int \alpha x^{-\alpha} \exp(-x^{-\alpha}) dx$$

Hence when

$$\sqrt{(N-1)(N-2)} < -h_{max} \int \alpha x^{-\alpha} \exp(-x^{-\alpha}) dx$$

the system is stable.

In the second example, we consider a coupled map with $\mathbf{H} = \mathbf{f}$. Under this assumption, $D\mathbf{H} = \mathbf{J}$ and the linearized equation [cf. Eq. (17)] reduces to

$$\mathbf{u}(t+1) = (\lambda/N + 1)\mathbf{J}(\mathbf{x}(t))\mathbf{u}(t). \tag{39}$$

The Lyapunov exponents for Eq. (39) are easily calculated analytically. Denoting them by $\mu_1(\lambda)$, $\mu_2(\lambda)$, $\ldots$, $\mu_M(\lambda)$, we have

$$\mu_i(\lambda) = h_i + \ln|\lambda/N + 1|, \quad i = 1, 2, \ldots, M. \tag{40}$$

For stability, we require $\mu_{max}(\lambda) = h_{max} + \ln|\lambda/N + 1| < 0$. In other words, the stability zone is defined by

$$|\lambda + N| < N \exp(-h_{max}) \tag{41}$$

The distance from the center of each Gershgorin disc to the boundary is easily calculated to be $\delta(b_{ii} - b_{ki}) = N\exp(-h_{max}) - |N + b_{ii} - b_{ki}|$ $(i = 1, \ldots, N, \ \ i \neq k)$. Thus the conditions of stability are

$$\sum_{j=1, j\neq i}^{N} |b_{ji} - b_{ki}| + |N + (b_{ii} - b_{ki})| < N \exp(-h_{max}), \tag{42}$$
$$i = 1, \ldots, N, \ \ i \neq k, \ \ k = 1 \text{ or } 2 \text{ or } \cdots \text{ or } N.$$

For each k from 1 to N, we obtain a set of sufficient stability conditions.

In [55], a simple stability bound for synchronized chaos in the case of symmetric coupling was obtained as

$$[1 - \exp(-h_{max})] < b_{ij} < [1 + \exp(-h_{max})], \quad \forall i, j. \tag{43}$$

As before, we see that Eq. 43 is equivalent to

$$\begin{cases} \max_{i,j} b_{i,j} & < & [1+\exp(-h_{max})] \\ \min_{i,j} b_{i,j} & > & [1-\exp(-h_{max})] \end{cases} \tag{44}$$

If we further $H_{\max} < 0$ and $b_{i,j} > 0$ then the second inequality in Eq. (44) is automatically fulfilled. Again we have three different behaviors of stability, depending on the distribution of $b_{i,j}$.

In summary, we have set up a general formalism to study the stability of synchronized states in coupled identical maps and ordinary differential equations[56]. We have also considered the often used linear coupling function for coupled maps and coupled ODEs and given analytical results in these cases. We have shown that known stability bounds can be derived from our more general results.

4 Synchronization of linear systems with delayed coupling

Thus far we have considered networks in which the interaction is instantaneous. In this section we study the effect of transmission delay. In order to derive analytical results we return to the linear system in Eq. (1) first considered by May (Section 2). Two cases of delay will be examined: discrete delay and distributed delay.

4.1 The case of discrete delay

We consider the effect of discrete time delay τ on the stability results [57] outlined in section 2. Let the equations of motion be

$$\dot{\mathbf{x}}(t) = -\mathbf{x}(t) + \mathbf{x}(t-\tau)\mathbf{B}^T \tag{45}$$

The decoupled eigenmode equation is

$$\dot{u}(t) = -u(t) + \lambda u(t-\tau) \quad \lambda \in \mathcal{C} \tag{46}$$

which represents a generalization of Pecora-Carrol's master stability equation. In this particular case it is possible to solve (46) analytically. The stability of the delay

differential equation (46) is determined by the characteristic equation

$$H(z) = z + 1 - \lambda e^{-z\tau} = 0 \tag{47}$$

where $u(t) = e^{zt},\ z \in \mathcal{C}$. If all the roots satisfy $Re(z) < 0$ then the solution is stable. The possibility of a change of sign of $Re(z)$ by way of $Re(z) = \infty$ is excluded by a theorem of Datko [58]. Hence all other sign changes of $Re(z)$ must occur at purely imaginary $z = i\omega,\ \omega \in \mathcal{R}_0^+$. Inserting $z = i\omega$ into (47) leads to the following transcendental equation:

$$H(\omega) = i\omega + 1 - \lambda e^{-i\omega\tau} = 0 \tag{48}$$

which identifies all possible instabilities. The solution to equation (48) can be understood geometrically as the intersection of the straight line $(i\omega + 1)/\lambda$ with the unit circle $e^{-i\omega t}$ plotted in the complex plane which is graphically illustrated in the cartoon of figure 4. The point or $\omega = 0$ defines the point S, from which the straight line originates for increasing ω. If S is within the unit circle, that is $\mid \lambda \mid^2 > 1$, then the straight line has always an intersection with the unit circle and hence a root of equation (48) is found. If S is outside of the unit circle, $\mid \lambda \mid^2 < 1$, then simple geometrical considerations show, that the slope of the straight line is always such that no intersection, and hence no instability, can occur.

Figure 4 nicely illustrates the conditions under which an instability exists, but does not give any for the size of the stability regimes. For this we return to the complex λ plane in Figure 1. It is easy to see in (47) that, for $Re(\lambda) = a = 1$ and $Im(\lambda) = b = 0$, we have $z = 0$ which corresponds to a change of stability. The point ($a = 1$ and $b = 0$) in the λ plane is also part of the boundary separating stable from unstable regions in Figure 1 for the undelayed system with $\tau = 0$. This fact is significant since it means that regardless of the delay τ the stability condition for Eq. (45) is at most as tight as that in Eq. (6). What is not known at this stage is what happens to the other part of the unit circle in figure 1 as τ increases. Intuitively it can be understood that the stability boundary changes as τ increases from zero and hence prescribes a two-dimensional surface in the three-dimensional space spanned by the parameters (a, b, τ). This critical surface is defined by equation (48) and can

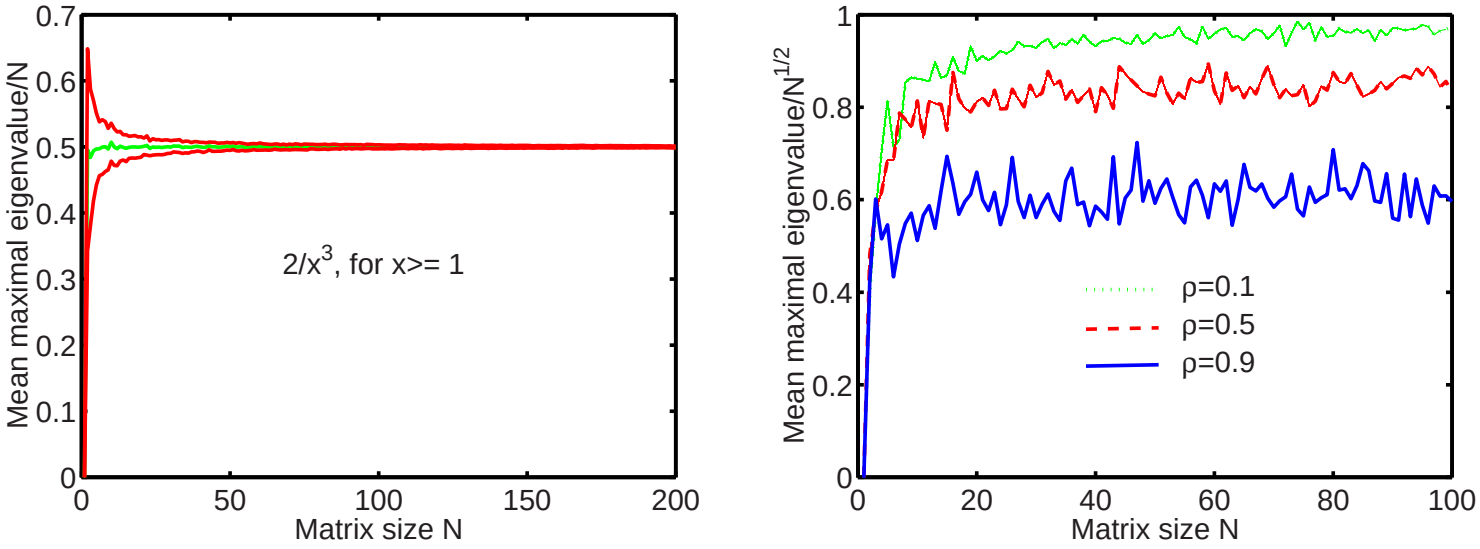

Figure 3: Left, mean maximal eigenvalue of $\mathbf{B}/N$ and mean maximal eigenvalue $\pm$ standard deviation of maximal eigenvalues vs. matrix size N. Right, mean maximal eigenvalue of $\mathbf{B}/\sqrt{N}$ vs. matrix size N for correlation coefficient $\rho = 0.1, 0.5, 0.9$.

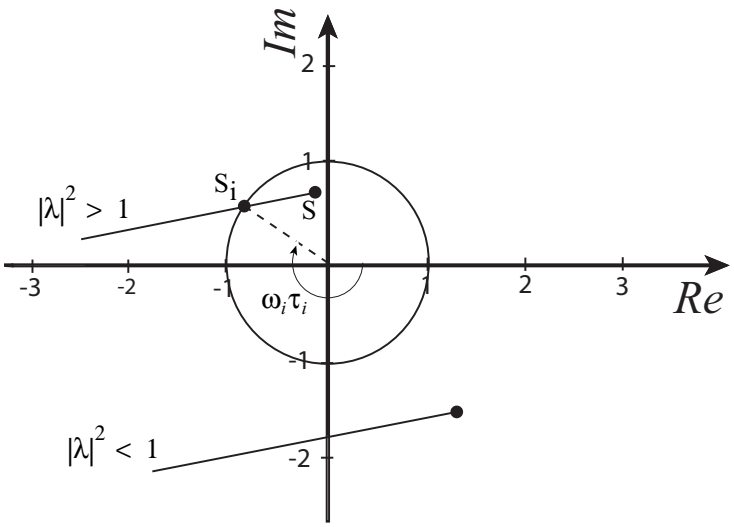

Figure 4: Visualization of the solution of the characteristic equation (48). If the point S is inside the unit circle, $\mid \lambda \mid^2 > 1$, then there is always an intersection point S_i and hence there may be an instability. If the intersection point S_i does not exist, $\mid \lambda \mid^2 < 1$, then the system will always remain stable.

be computed analytically. After some straightforward manipulations of equation (48), the condition for the critical delay, at which a change in stability may occur, can be written as

$$\tan \omega\tau = \frac{b - a\omega}{a + b\omega} \tag{49}$$

and the critical frequency is identified as

$$\omega^2 + 1 = (a^2 + b^2) \tag{50}$$

From these two equations the critical surface $\tau = g(a, b)$ is given by

$$\tau = \frac{-1}{\sqrt{\mid \lambda \mid^2 -1}} \tan^{-1} \frac{a\sqrt{\mid \lambda \mid^2 -1} - b}{a + b\sqrt{\mid \lambda \mid^2 -1}} \tag{51}$$

Equation (51) defines clockwise and counterclockwise oriented spirals, the so-called Archimedean spirals [59]. The segments of the spirals with the smallest delay contribute to the actual critical surface, which defines the first instability and is illustrated in figure 5. Similar results given implicitly in polar coordinates may be found in [59]. The half volume $a > 1$ contains solutions which are always unstable. If $a < 1$, then the cylinder defined by $\mid \lambda \mid^2 = a^2 + b^2 = 1$ contains solutions which are stable for all delays τ. Outside of this cylinder the size of the stability region depends on τ. Cross sections for various values of τ are shown in Figure 6. For $\tau = 0$, the stability region is the entire half plane $a < 1$. For non-zero τ, the stability regime is finite and teardrop-shaped. The stability region decreases and approaches the stability cylinder defined by $a^2 + b^2 = 1$ for increasing values of τ. The nature of the stability change for increasing τ is determined uniquely by the sign of $dRe(z)/d\tau$ [57] which can be written as

$$\frac{dRe(z)}{d\tau} = -Re[\frac{\partial H/\partial \tau}{\partial H/\partial z}] = \omega^2 / \mid D \mid^2 > 0 \tag{52}$$

where $D = e^{z\tau} + \lambda\tau$. This means that as τ increases across the critical surface from below, the system always becomes unstable.

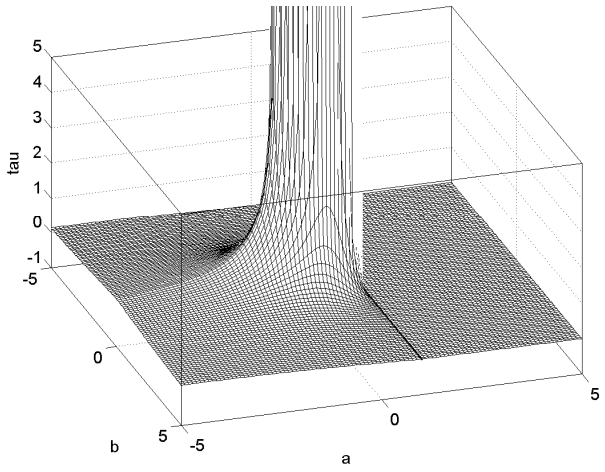

Figure 5: The critical surface given in (51) defines the minimal critical delay values τ at which the system (1) becomes unstable. For $a > 1$, all solutions are unstable. For $a < 1$, only the solutions below the critical surface are stable. All solutions above the critical surface are unstable.

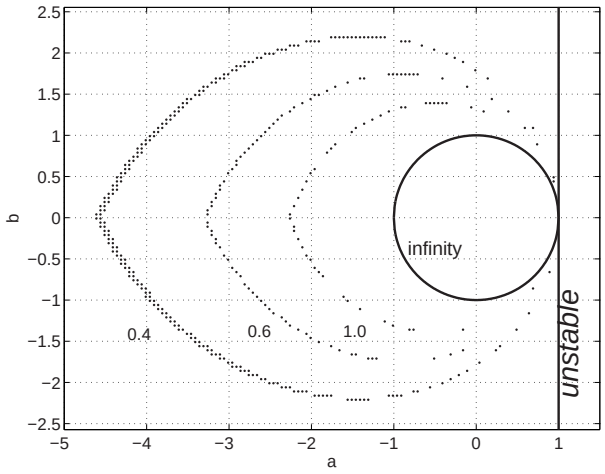

Figure 6: Cross sections of the critical surface defined by (51) are shown for the delay values $\tau = 0, 0.4, 0.6, 1.0$ and ∞. For $\tau = 0$, the entire left half plane, $a < 1$, is the stability region, whereas for $\tau = \infty$ it is the unit circle centered at the origin. For intermediate values, the stability region decreases as τ increases.

4.2 The case of distributed delay

In most real-world scenarios, the delay will not be sharply defined, but distributed. Here we consider the effect of the distributed delay on the stability results above. Let the equations of motion be

$$\dot{x}_i = -x_i + \sum_{j=1}^{N} b_{ij} \int_0^\infty f(\tau', d) x_j(t - \tau')\, d\tau' \tag{53}$$

The real-valued kernel function $f(\tau', d) = f(\tau' - \tau, d)$ with mean delay $\tau \in \mathcal{R}_0^+$ captures the continuous distribution of delay values and reduces to Dirac's delta function $\delta(\tau' - \tau)$ when its width d approaches zero. Normalization is guaranteed by $\int_0^\infty f(\tau', d)d\tau' = 1$ and $\tau' \in \mathcal{R}_0^+$ ensures causality. In matrix form Eq. (53) is

$$\dot{\mathbf{x}} = -\mathbf{x} + \int_0^\infty f(\tau', d)\mathbf{x}(t - \tau')\, d\tau' B^T \tag{54}$$

The eigenmode equation is

$$\dot{u} = -u + \lambda \int_0^\infty f(\tau', d) u(t - \tau')\, d\tau', \quad \lambda \in \mathcal{C} \tag{55}$$

The stability of the integral-differential equation (55) is determined by the characteristic function

$$H(z) = z + 1 - \lambda e^{-z\tau} F(z) = 0 \tag{56}$$

where the function $F(z) = F(z, d)$ is defined as $F(z) = \int_0^\infty f(\tau', d)e^{-z\tau'}d\tau'$. If all the roots satisfy $Re(z) < 0$ where $u = e^z$, $z \in \mathcal{C}$ then the solution of (53) will be stable. It is important to note that, for $\lambda = a + ib$ in Eq. (56), setting $a = 1$ and $b = 0$ again leads to $z = 0$ which corresponds to a change of stability. Thus, the disk of stability can be at most the unit circle. To investigate the critical surface we let $z = i\omega$, $\omega \in \mathcal{R}_0^+$. Note that our results are exact so far, but it is worth to consider the following constraint to gain some intuition on $F(z)$: If the mean delay value τ is sufficiently far away from zero, that is $\tau \gg d$, then $F(z) = \int_0^\infty f(\tau', d)e^{-z\tau'}d\tau' \approx \int_{-\infty}^\infty f(\tau', d)e^{-z\tau'}d\tau'$. Under this mild condition and with $z = i\omega$, the function $F(z) = F(\omega) = F_1(\omega) + iF_2(\omega)$ becomes identical with the complex-valued Fourier transform of the kernel function. Alternatively, we can

always extend the defining integral range of $F(z)$ from $-\infty$ to ∞ by formally setting $f(\tau', d) = 0$ for $\tau' < 0$. The resulting expression for $F(z)$ is exact, but has the disadvantage that it cannot be interpreted as the Fourier transform of the original (and in most cases well-known) delay distribution $f(\tau', d)$, but rather is the Fourier transform of its truncated form which misses its left tail for $\tau' < 0$. Again, in most applications there will be no noticeable difference in the interpretations.

To continue our discussion of the critical surface, we insert $z = i\omega$ into (56) and obtain

$$\Gamma(\omega) = \tan \omega\tau + \frac{F_1(\omega)(a\omega - b) - F_2(\omega)(a + b\omega)}{F_1(\omega)(a + b\omega) + F_2(\omega)(a\omega - b)} = 0 \tag{57}$$

and

$$\omega^2 + 1 = \mid \lambda \mid^2 \mid F(\omega) \mid^2 \tag{58}$$

Solving for ω we will have an equation that determines the critical surface in the (a, b, τ) space. Unfortunately, for a general delay kernel, we are not able to obtain explicit formulas for the critical surface. However, it turns out that all positive definite and normalizable functions $f(\tau', d)$ result in a critical surface which is bounded from below by the critical surface of the discrete delay. As a consequence, the discrete delay is the most destabilizing case. Or, in other words, as the width d of the time delay distribution increases, the less unstable the system becomes. This can be understood as follows: The frequency ω is obtained from (58) as the intersection of the two curves $y_1(\omega) = \omega^2 + 1$ and $y_2(\omega) = \mid \lambda \mid^2 \mid F(\omega) \mid^2$ which are illustrated in Figure 7 for $\lambda = 1$. In particular, $F(\omega)$ has the property $F(\omega = 0) = \int_{-\infty}^{\infty} f(\tau')d\tau' = 1$ and

$$\begin{aligned} \mid F(\omega \neq 0) \mid &= \mid \int_{-\infty}^{\infty} f(\tau') e^{-i\omega\tau'} d\tau' \mid \\ \leq \int_{-\infty}^{\infty} \mid f(\tau') \mid \underbrace{\mid e^{-i\omega\tau'} \mid}_{=1} d\tau' &\leq \int_{-\infty}^{\infty} f(\tau') d\tau' = 1 \end{aligned} \tag{59}$$

Hence $\mid F(\omega) \mid$ will always be smaller or equal for all ω. The equality sign holds for the discrete delay case, $\lim_{d \to 0} F(\omega, d) = 1 \ \forall \omega$. Taken together with the fact that $y_1(\omega)$ is a positive definite and monotonically increasing curve, it follows that the

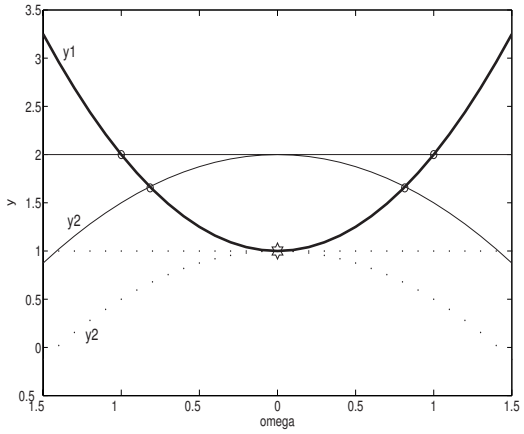

Figure 7: Cartoon illustrating the intersection of y_1 (solid bold line) and y_2 (dotted line) for the critical case of $\lambda = 1$. The horizontal dotted line illustrates $F(0) = 1$. For this situation, there is only one intersection identified by the star for $\omega = 0$. For $\lambda > 1$, y_2 and the horizontal line shift upwards (as illustrated by the thin solid lines). Both, y_2 and the horizontal line, have an intersection with y_1, but y_2 always at a lower value of ω than for the horizontal line. For $\lambda < 1$, y_2 shifts downwards and there is no intersection between y_1 and y_2 and hence no instability.

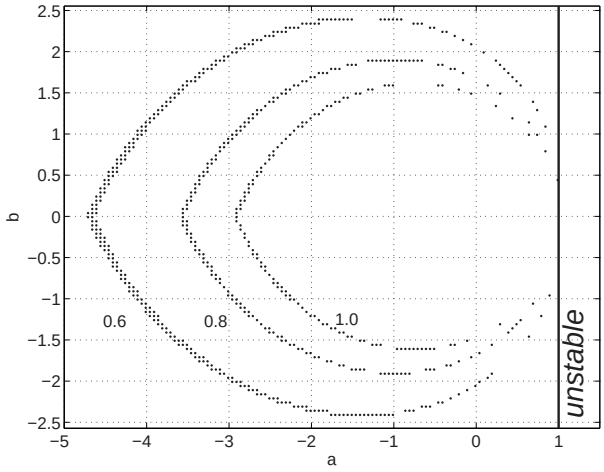

Figure 8: Cross sections of the critical surface are shown for the values $\omega = 1, 0.8, 0.6$ at a time delay of $\tau = 0.7$. It is evident that the stability area increases with decreasing ω.

discrete delay case results in an intersection of the two curves $y_1(\omega)$ and $y_2(\omega) =\mid \lambda \mid^2$ at the highest frequency ω. Every other distribution function will have its intersection of $y_1(\omega)$ and $y_2(\omega) =\mid \lambda \mid^2 \mid F(\omega) \mid^2 <\mid \lambda \mid^2$ at a smaller frequency ω. To understand the effects of the decreased frequency on the critical surface, we study $d\tau/d\omega$ and consider first a symmetric distribution function $f(\tau', d) = f(\tau' - \tau, d) = f(\tau' + \tau, d)$. In this case the Fourier transform $F(\omega) = F_1(\omega)$ is real valued with $F_2(\omega) = 0$. Then Eq. (57) becomes identical to (49) as discussed in the discrete delay case. We characterize the change of the critical surface by

$$\frac{d\tau}{d\omega} = -\frac{\partial\Gamma/\partial\omega}{\partial\Gamma/\partial\tau} = -\tau/\omega - \frac{(a^2+b^2)\cos^2\omega\tau}{\omega(a+b\omega)^2} < 0 \tag{60}$$

for all $\omega, \tau \in \mathcal{R}_0^+$. As a consequence, any decrease in ω will result in an increase of the stability region in the complex λ plane and hence a stabilization of the system (53) compared to the discrete delay case. This general result is illustrated in Figure 8 for symmetric distribution functions $f(\tau', d)$. For arbitrary distribution functions, $F(\omega) = F_1(\omega) + iF_2(\omega)$ is generally complex-valued and results in a rotation of the critical surface around the vertical axis at $a = 1$ and $b = 0$ as described by (57). In this case, a lengthy calculation shows that all our results will remain valid for general distribution functions, if $F_1'(\omega)F_2(\omega) - F_2'(\omega)F_1(\omega) \geq 0$ holds where the prime denotes the derivative with respect to ω. Under this sufficient condition, the

critical surface for the discrete delay case defines the lower bound for the critical surfaces of arbitrary distribution functions.

Finally, the nature of a stability change for increasing τ is determined uniquely by the sign of $dRe(z)/d\tau$ [57] which is obtained from (56)

$$\frac{dRe(z)}{d\tau} = -Re[\frac{\partial H/\partial \tau}{\partial H/\partial z}] \tag{61}$$

After some algebra we obtain

$$\frac{dRe(z)}{d\tau} = \frac{\omega^2}{\mid D \mid^2} - \frac{\omega(\omega^2+1)}{\mid D \mid^2} Re[\frac{\partial}{\partial \omega} \ln F(\omega)] \tag{62}$$

where

$$D = 1 + \lambda\tau e^{-z\tau} F(z) - \lambda\tau e^{-z\tau} F'(z) \tag{63}$$

and $F'(z) = \partial F(z)/\partial z$. If $dRe(z)/d\tau$ is greater than zero, then the system becomes unstable as τ is increased from below the critical surface to above it. Otherwise we have a stabilizing bifurcation.

In summary, for both discrete and distributed delay cases, the point $a = 1$ and $b = 0$ separates stability from instability. This means that the stability disk for the random coupling matrix is at most the unit circle. On the other hand, it is clear that, for the discrete delay case, the unit circle remains stable for all delays. The distributed delay results in critical surfaces that lie above the critical surface of the discrete delay case. This means that the unit circle is again stable for all possible delays for the distributed delay case. These observations lead to the remarkable result that May's stability condition Eq. (6) remains intact despite the fact that the introduction of time delay clearly reduces the regions of stability.

4.3 Examples

For concreteness we consider two explicit examples to generate some insights into the problem.

4.3.1 Gaussian distribution

The kernel function is taken to be the Gaussian function

$$f(\tau' - \tau, d) = \frac{1}{\sqrt{2\pi d^2}} e^{-(\tau'-\tau)^2/(2d^2)} \tag{64}$$

and is fully symmetric with regard to τ. Hence we may apply (49) to identify the critical surface parametrized by ω. The frequency is obtained from (58) as $\omega^2 = (\mid \lambda \mid^2 -1)(1 + d \mid \lambda \mid^2)^{-1}$ and is smaller for increasing width d. As a consequence, the critical delays for the distributed case will be greater than in the discrete delay case. The nature of the instability at the critical surface is destabilizing for the Gaussian distribution function, because it follows from (62) that $dRe(z)/d\tau = \omega^2 \mid D \mid^{-2} (1 + d(\omega^2 + 1)) > 0$ and hence results in destabilization. Note that D has been defined in (63).

4.3.2 Uniform distribution

The symmetric uniform distribution is defined as $f(\tau' - \tau, d) = (2d)^{-1}$ for $-d \leq \tau' - \tau \leq d$ and zero otherwise. The critical frequency is obtained from $\omega^2 = (\mid \lambda \mid^2 -1)(1 + d^2 \mid \lambda \mid^2 /3)^{-1}$ for small d and also results in smaller frequencies ω for increasing width d, and hence again in greater critical delays than the discrete delay case. The uniform distribution results in destabilization as τ increases through the critical surface since $dRe(z)/d\tau = \mid D \mid^{-2} (\omega^2 + (\omega^2 + 1)(1 - \omega d/\tan \omega d)) > 0$ for $\omega d \in [0...\pi/2]$. D has been defined in (63).

5 Applications to Neuroscience

From the foregoing discussion we see that there are essentially two steps involved in establishing the stability of synchronized solutions in randomly coupled systems. First, we find the stability region by employing the master stability function. Second, we find constraints on the random coupling matrix based on the stability region. In simple examples, both steps can be done analytically as we have seen earlier. But for problems arising from applications often numerical methods are needed. In this

section we consider models in Neuroscience[60, 61, 63, 64]. In particular, networks of Hodgkin-Huxley models are investigated. This example is typical of real world problems where both nonlinearity (Section 3) and transmission delay (Section 4) are inevitable elements of the system.

5.1 Models

For a description of the neuronal dynamics we use the Hodgkin-Huxley (HH) model[65],

$$\dot{V} = \frac{1}{C}(I_{ion}(V, m, h, n) + I_{ext}) \tag{65}$$

$$\dot{m} = \frac{m_\infty(V) - m}{\tau_m(V)}, \quad \dot{h} = \frac{h_\infty(V) - h}{\tau_h(V)}, \quad \dot{n} = \frac{n_\infty(V) - n}{\tau_n(V)} \tag{66}$$

where C is the membrane capacitance, V is the membrane potential,

$$I_{ion}(V, m, h, n) = -g_{Na}m^3h(V - V_{Na})dt - g_kn^4(V - V_k)dt - g_L(V - V_L)$$

is the total ionic current, and I_{ext} is an externally applied current which we will assume to be constant. For a detailed definition and values of the parameters in the model at a temperature 6.3° C, we refer the reader to [65, 66]. In the following, we will indicate the 'gate variables' collectively by the vector $s = (m, h, n)$, and put $C = 1$.

For $I_{ext} < I_1 \approx 6\ \mu\text{A/cm}^2$ the system (65)-(66) has a globally attracting fixed point: if excited, the neuron fires a single action potential and then returns to the resting state. Periodic solutions arise at $I_{ext} = I_1$, through a saddle-node bifurcation. For $I_1 < I_{ext} < I_2 \approx 9.8\ \mu\text{A/cm}^2$, the system has two attractors, a fixed point and a limit cycle, and the neuron starts showing oscillations of small amplitude around the resting potential. At $I_{ext} = I_2$ the unstable branch of the periodic solutions dies through an inverse Hopf bifurcation, and for $I_{ext} > I_2$ the system has only one attractor which is a limit cycle. In this region, the neuron fires repetitively.

5.1.1 Diffusive coupling

We start by considering two identical neurons, represented by the variables V_i, s_i, $i = 1, 2$, coupled linearly via their membrane potentials. This type of coupling, usually referred to in the literature as *diffusive* coupling, is appropriate for describing an electrical synapse. For the sake of simplicity, we consider symmetrical coupling. The system is described by

$$\dot{V}_i = I_{ion}(V_i, s_i) + I_{ext} + \epsilon\,[V_j(t-\tau) - V_i] \quad i, j = 1, 2 \quad j \neq i \tag{67}$$

where ϵ is the coupling strength, $\tau \geq 0$ is the time delay in the interaction, and the gate variables follow equations similar to Eq. (66).

A *synchronous state* for our system, is a solution of Eq. (67) such that

$$(V_1(t), s_1(t)) = (V_2(t), s_2(t)) \tag{68}$$

for all times t. This state lies on the *synchronization* manifold $(V_1, s_1) = (V_2, s_2)$, which is invariant due to the symmetry of the equations. Given asymmetric initial conditions, we say that the system *synchronizes* if Eq. (68) holds asymptotically. It follows from the definition that, for a synchronous state, we have

$$\begin{cases} \dot{V} &= I_{ion}(V, s) + I_{ext} + \epsilon\,[V(t-\tau) - V] \\ \dot{s} &= \frac{s_\infty(V) - s}{\tau_s(V)} \end{cases} \tag{69}$$

In the absence of delay, the equations above reduce to Eq. (65)-(66), thus, for any value of the bifurcation parameter I_{ext}, each neuron in a synchronous state will behave as if the interaction were absent. In particular, for $I_{ext} > I_2$, the two coupled neurons, once synchronized, will fire periodically as if they were isolated. In the presence of delay, on the other hand, the behavior of a neuron entrained in a synchronous state can be radically different from that of a neuron in isolation. It can be shown that single units displaying a chaotic behavior can be recruited into synchronized periodic oscillations, or periodic oscillators can exhibit synchronized chaos when coupled.

For the synchronous state to be stable, all motions transverse to the synchronization manifold must asymptotically damp out. To examine this, we first reformulate

the problem using a more precise notation. By defining $\mathbf{X}^i = (V_i, m_i, h_i, n_i)$ and $\epsilon_1 = (\epsilon_1, 0, 0, 0)$, the system is rewritten as

$$\dot{\mathbf{X}}^i = \mathbf{F}(\mathbf{X}^i) + \epsilon_{\mathbf{1}} \cdot (\mathbf{X}^j(t-\tau) - \mathbf{X}^i) \quad i, j = 1, 2 \quad j \neq i \tag{70}$$

and the synchronous state $\mathbf{X}(t)$ is defined as a solution of

$$\dot{\mathbf{X}} = \mathbf{F}(\mathbf{X}) + \epsilon_{\mathbf{1}} \cdot (\mathbf{X}(t-\tau) - \mathbf{X}) \tag{71}$$

where $\mathbf{F}$ is defined by Eq. (69). We now introduce the transverse vector $\mathbf{X}_\perp = \mathbf{X}^2 - \mathbf{X}^1$, and linearize the system (70) around the synchronous state, to obtain

$$\dot{\mathbf{X}}_\perp = \mathbf{J}(\mathbf{X}(t)) \cdot \mathbf{X}_\perp - \epsilon_{\mathbf{1}} \cdot (\mathbf{X}_\perp(t-\tau) + \mathbf{X}_\perp) \tag{72}$$

where the matrix $\mathbf{J} = D\mathbf{F}(\cdot)$ is the Jacobian of $\mathbf{F}$. The stability of the synchronous state is now related to the Lyapunov exponents associated with the system (72)[67]. Because of the delay term, the system considered is a functional differential equation with an infinite number of Lyapunov exponents. The synchronous state is stable if all the Lyapunov exponents are negative. This condition is ensured if the *maximum* Lyapunov exponent can be calculated and it is shown to be negative.

5.1.2 Pulse coupling

Although numerous examples of electrical synapses have been described in the nervous system of invertebrates and lower vertebrates, the most widespread interaction mechanism among the neurons in the mammalian brain relies on pulse-like release of neurotransmitters following action potentials[68]. In order to apply the approach described above to this case, the pulse-like interaction must be first put into a convenient mathematical form. In particular, the interaction term must be expressed as a function of the variables of the presynaptic neuron. Hence we consider of the following model,

$$\dot{V}_i = I_{ion}(V_i, s_i) + I_{ext} + \epsilon \cdot \delta(V_j(t-\tau) - \bar{V}) \cdot \Theta(m_j(t-\tau) - \bar{m}), \tag{73}$$

where $\Theta(\cdot)$ is the Heaviside function, and $\bar{m}$ is a suitably chosen constant. Due to the m-dependent factor in the interaction term, it is possible to select either the

upward or the downward threshold crossing event, as it is evident from considering a projection of the spike trajectory on the $V-m$ plane. In particular, the interaction term in Eq. (73) will differ from zero only when the membrane potential crosses the threshold from below.

The system is formulated as follows,

$$\dot{\mathbf{X}}^i = \mathbf{F}(\mathbf{X}^i) + \sum_{j=1}^{2} G_{ij}\mathbf{H}(\mathbf{X}^j(t-\tau)) \quad i = 1,2 \tag{74}$$

where $\mathbf{X}^i = (V_i, s_i), i = 1, 2$, $\mathbf{G} = [G_{ij}]$ is the coupling matrix given by

$$G_{11} = G_{22} = 0 \quad G_{12} = G_{21} = \epsilon_1, \tag{75}$$

and the interaction term is given by

$$\mathbf{H}(\mathbf{X}) = (H_1, 0, 0, 0) = \big(\delta(X_1 - \bar{X}_1)\Theta(X_2 - \bar{X}_2), 0, 0, 0\big) \tag{76}$$

Linearizing the motion around the synchronous state, we obtain in the transverse direction,

$$\dot{\mathbf{X}} = \mathbf{F}(\mathbf{X}) + \epsilon_1 \cdot \mathbf{H}(\mathbf{X}(t-\tau)) \tag{77}$$

$$\dot{\mathbf{X}}_\perp = \mathbf{J}(\mathbf{X}(t)) \cdot \mathbf{X}_\perp - \epsilon_1 \cdot D\mathbf{H}(\mathbf{X}(t-\tau)) \cdot \mathbf{X}_\perp(t-\tau) \tag{78}$$

Note that, in this case, the synchronous state depends on the coupling even in the absence of delay. Also, because of the nature of the interaction, we have to deal with singular terms in $D\mathbf{H}$. In particular we have

$$\frac{\partial H_1}{\partial X_1} = \delta'(X_1 - \bar{X}_1)\Theta(X_2 - \bar{X}_2), \tag{79}$$

and

$$\frac{\partial H_1}{\partial X_2} = \delta(X_1 - \bar{X}_1)\delta(X_2 - \bar{X}_2), \tag{80}$$

where δ' is the derivative of the delta function in the sense of distributions. Although both terms are highly singular, fortunately a numerical solution of the linearized system is still possible. When a forward Euler scheme is used to solve (77)-(78), the two 'hard' terms are integrated as

$$A = \int_t^{t+\Delta t} \Theta(m(t'-\tau) - \bar{m})\delta'(V(t'-\tau) - \bar{V})V_\perp(t'-\tau)dt', \tag{81}$$

and

$$B = \int_t^{t+\Delta t} \delta(m(t'-\tau) - \bar{m})\delta(V(t'-\tau) - \bar{V})m_\perp(t'-\tau)dt' \tag{82}$$

Let us consider the term A first. Since the system crosses the m-threshold, $\bar{m}$, and the V- threshold, $\bar{V}$, for different values of t, we have that for all the intervals containing the zeros of the argument of δ', the rest of the integrand is regular. In particular, for all the intervals containing the upward crossing times we will have

$$A = \int_t^{t+\Delta t} \delta'(V(t'-\tau) - \bar{V})V_\perp(t'-\tau)dt' = -\frac{\dot{V}_\perp(t_i)}{|\dot{V}(t_i)|} I_{[t+\tau,t+\tau+\Delta]}(t_i)$$

where $\{t_i\}$ indicates the upward crossing times previous than t, and I is the indicator function. On the other hand, during the downward crossing events we will have $A = 0$.

As for term B, it is easy to show that, once the 'driving' system $\mathbf{X}(t)$ has settled on the attractor, the integrand is always null, so we can assume $B = 0$ for all times during integration.

5.2 Results

All the differential systems have been integrated numerically using a forward Euler scheme with a time step of 10 μs. A standard technique to calculate the largest Lyapunov exponent, $\lambda_\perp$, consists in averaging the exponential growth rate of the vector $\mathbf{X}_\perp$ along the trajectory [69]. Alternatively, as suggested in [70], the finite time estimate

$$\hat{\lambda}_\perp(T) = \frac{1}{T}\log|\mathbf{X}_\perp(T)| \tag{83}$$

can be used, provided T is a reasonably long time. However, we found this procedure to be prone to errors, because of the oscillating behavior of $\log|\mathbf{X}_\perp(t)|$. Instead, a more reliable estimate is obtained by considering the function

$$\xi(t) = \frac{1}{t}\int_0^t \log|\mathbf{X}_\perp(t')|\ dt'$$

Indeed, we have asymptotically

$$\xi(t) = const. + \frac{\lambda_\perp}{2}t + O(\frac{1}{t})$$

from where the maximum Lyapunov exponent can be estimated.

5.2.1 Diffusive coupling

For the case of diffusive coupling, we have considered a range of values for the applied current stimulus $I_{ext} = 7, 10, 15, 20\ \mu\text{A/cm}^2$. For all these values, the isolated neurons fire periodically. Simulation results show that $\lambda_\perp$ is always negative on the semi-axis ($\tau = 0,\ \epsilon > 0$), regardless of the amplitude of the current stimulus considered (see Fig. 9). Therefore, two identical HH neurons with symmetrical coupling will always synchronize in the absence of delays, no matter how small the coupling is. This result is consistent with what was shown in [71]. As expected, $|\lambda_\perp|$ increases monotonically with ϵ, indicating that the system synchronizes more rapidly with stronger coupling.

The (ϵ, τ) space is characterized by a predominance of stable solutions. However, the plot of Fig. 9 reveals three distinct regions (left panel, Fig. 9), which correspond to different behaviors of the solutions of the coupled system (67). Direct simulations revealed that in the region at the bottom of each graph, the synchronous state is represented by ordinary oscillations, and that this state is globally attractive. Therefore, in this region, two neurons will eventually synchronize, regardless of their initial phase. However, the synchronous state, and its stability, change with τ. In particular, when τ is increased above the first boundary line, the amplitude of the limit cycle on the synchronous manifold is suddenly reduced, and we observe the phenomenon of oscillation death (not shown). In order to display this behavior, the neuron must still have a stable resting state, albeit with a small basin of attraction. Therefore, oscillation death will only be observed in the region of bistability $I_1 < I_{ext} < I_2$. Note that, because of the term $-\epsilon V(t)$, the region of bistability of the model with self-interaction, is different from that of the isolated model, thus explaining why the quenched oscillations can be observed also in the other cases considered here. In the region between the two boundary lines, this state is locally attractive for the dynamics of the complete system, thus we see coupled neurons reciprocally suppressing their oscillations. Occasionally, depending on the initial conditions and the choice of the parameters, we observed the coupled system desynchronizing and settling in an anti-phase locked oscillatory state (not shown). The

'hot-spot' near the upper left corner of Fig. 9 is indicative of a different attractor on the synchronous manifold. In this case, the time delay is such that the current pulse, due to the self-interaction, is delivered too late to switch the system to the resting state, yet too early to anticipate the onset of the next spike. However, we found that these oscillations are very easily destabilized, and the complete system is attracted to the anti-phase locked state. Finally, in the region above the upper boundary line, the synchronous state is again oscillatory, although the firing rate is now almost twice as much as that of the isolated neurons. This is due to the self-interaction pulse which follows each spike, which now is delivered sufficiently late, and with a sufficient amplitude, to overcome refractoriness and anticipate the occurrence of the following spike.

In Fig. 10 we depicted the period of the oscillations, T, observed by simulating the coupled system. The figure has to be viewed together with Fig. 9. Below the unstable region, the values reported correspond to the period of the synchronous oscillations. In the region (middle) where the synchronous state is not stable, the observed period is that of anti-phase locked solutions. The points where $T = 0$ (that appear as dark blue 'holes' in the graph), mark the values of the parameters for which quenched oscillations were observed. In the upper region, a mixed phenomenon is observable, with the seemingly random occurrence of synchronized and anti-phase locked states. This plot shows clearly the sudden drop of the period across the lower boundary line, which marks the onset of an attractive anti-phase locked oscillatory state in the entire system's phase space. The predominance of solutions with $T \neq 0$ demonstrates that although quenched oscillations (the 'holes' at $T = 0$) are locally stable in this region, the anti-phase locked state has a much larger basin of attraction. For longer delays, we observe instead a mixture of two phases corresponding to synchronous, and anti-phase locked oscillations, which indicates that the actual synchronization, for these values of the coupling parameters, is largely dependent on the initial conditions of the system.

In summary we presented a systematic study for two diffusively coupled HH neurons, in terms of the Lyapunov exponent and confirmed by direct simulations. It is generally easy to synchronized two neurons due to the nature of interactions. We

also presented a Matlab program (http://www.informatics.sussex.ac.uk/users/er28/synchronization/) to demonstrate the results presented here.

5.2.2 Pulse coupling

Fig. 11 upper panel shows the maximum transverse Lyapunov exponent of the system (77)-(78), as a function of (ϵ, τ). Here we considered also negative values of ϵ to represent a reciprocal inhibitory coupling.

Fig. 11 bottom panel also shows two 'sections' at $\epsilon = -4$ mV and $\epsilon = 4$ mV. In order to validate these results, we considered the behavior of the solutions of the system (77)-(78) for different values of (ϵ, τ). First, we set arbitrary initial conditions on the synchronous manifold, $\mathbf{X_1} = \mathbf{X_2}$, and let the system settle onto the attractor. After a transient, the system is displaced out of the synchronous manifold by an instantaneous perturbation on V_1, $V_1 \to V_1 + \delta V$, and then it is let to evolve unperturbed. In Fig.12 we reported some of the calculated trajectories projected onto the (V_1, V_2) plane. These plots illustrate the qualitatively distinct behaviors that are observed for different values of ϵ and τ, including synchronization, phase locking, anti-phase locking and possible chaos. For all the cases considered, the observed behavior was found to be consistent with the calculated Lyapunov exponent.

We observed that, when the synchronous state is stable, the type of attractor that lies outside its basin of stability depends on the sign of the coupling. In particular, if the coupling is positive, the solution is attracted onto a phase-locked state (Fig.12 upper right), whereas for negative coupling a chaotic attractor seems to be present (see Fig.12 bottom right). Also we noticed that the two branches around the minimum in Fig. 12 (bottom left) correspond to a change in the structure of the attractors around the synchronous manifold. In particular, for the left branch the synchronous state is very stable, as if it was the only attractor in the whole space, while for the right branch the stability of the synchronous state is lost by being attracted onto a seemingly chaotic state.

Finally, we can now address the issue of whether inhibitory or excitatory inter-

actions can facilitate synchronization. In the literature, it is often reported that inhibitory, but not excitatory interactions, can synchronize two neurons, a result that is based upon analysis of the leaky integrate and fire model[72, 73]. Our results tell us that, for the HH model, *both* excitatory and inhibitory interactions can synchronize neuronal activity. Figure 13 (left) does show that in terms of the magnitude of the Lyapunov exponent, inhibitory interactions have a more negative value and so it is more stable in this sense, in agreement with results in the literature. However, when we look at the sign of the Lyapunov exponent, we have a totally different scenario. With excitatory interactions the regions in which the Lyapunov exponent is negative are bigger than that with inhibitory interactions (Fig. 13 (right)). In fact, the averaged sign(λ) is always positive when the interaction is negative.

5.2.3 Synchronization in time-delayed networks

Now we consider a system containing an arbitrary number of neurons with general coupling topologies. This can be done following the scheme used by Pecora and Carroll [10]. Given a system of N interacting HH neurons, with coupling matrix $\mathbf{G}$,

$$\dot{\mathbf{X}}^i = \mathbf{F}(\mathbf{X}^i) + \sum_j G_{ij}\mathbf{H}(\mathbf{X}^j(t-\tau)) \tag{84}$$

the stability problem, originally formulated in a $4 \times N$ dimensional space, can be reduced to the study of the system

$$\dot{\xi}(t) = \mathbf{J}(\mathbf{X}(t))\xi(t) + (\alpha + i\beta)D\mathbf{H}(\mathbf{X}(t-\tau))\xi(t-\tau) \tag{85}$$

where $\alpha + i\beta$ is an eigenvalue of $\mathbf{G}$, in general complex-valued, and ξ is a 4 dimensional perturbation vector. To ensure that the synchronized state $\mathbf{X}^i = \mathbf{X}$ is a solution of the dynamics, we require that

$$\sum_j G_{ij} = 0, \quad i = 1, \cdots N. \tag{86}$$

By separating ξ into the real part ξ_r and imaginary part ξ_i, we get

$$\dot{\xi}_r = \mathbf{J}(\mathbf{X})\xi_r + \alpha D\mathbf{H}(\mathbf{X}_\tau)\xi_{r\tau} - \beta D\mathbf{H}(\mathbf{X}_\tau)\xi_{i\tau} \tag{87}$$

$$\dot{\xi}_i = \mathbf{J}(\mathbf{X})\xi_i + \alpha D\mathbf{H}(\mathbf{X}_\tau)\xi_{i\tau} + \beta D\mathbf{H}(\mathbf{X}_\tau)\xi_{r\tau} \tag{88}$$

where $\xi_{r\tau} = \xi_r(t-\tau)$ and $\xi_{i\tau} = \xi_i(t-\tau)$. For a given value of τ, we can consider α, β as parameters, and estimate the maximum Lyapunov exponent $\lambda_{\perp,max}$ from Eqs. (87) and (88). This function is known as the master stability function, and defines a region of stability of the synchronous oscillations in terms of the eigenvalues of the coupling matrix. Given a particular network topology and a value of the time delay, the synchronous state will be stable if, and only if, all the eigenvalues of the coupling matrix lie in the region of stability indicated by the master stability function.

The plots of Fig. 14 show the results obtained for the diffusive coupling case, for an external stimulus of $I_{ext} = 10\ \mu\text{A/cm}^2$ and different values of the delay. The stability region becomes smaller as the delay increases. It is interesting to compare the results in the current subsection with that in Subsection 5.2.1. It is easily seen that we have two eigenvalues for two HH models with diffusive coupling: one is $\alpha = -2\epsilon, \beta = 0$ and the other is $\alpha = 0, \beta = 0$. To apply the results in the current subsection to the case in this subsection, we see that the second eigenvalue lies on the boundary of the stable and unstable region. Nevertheless, a more detailed analysis tells us that in fact the results can not be applied to the cases considered in Subsection 5.2.1. The interaction term in Subsection 5.2.1 does not vanish, but it is zero due to the constraint (86) for the system (84). Of course, the results presented in Fig. 14 are general enough for an arbitrary interaction matrix satisfying the constraint (86).

In Fig. 15 we depicted the results for the pulse coupling case, obtained for the same values of I_{ext} and τ as for the diffusive coupling case above. Again it is worth noting that the dynamics considered here actually differ from that considered in the previous subsection, since we require that $\sum_j G_{ij} = 0$. Since real neurons are either excitatory or inhibitory, we have that, for fixed j, G_{ij} must have the same sign, either positive or negative, for all i. However, for a system of two neurons, it is impossible to implement such a coupling scheme if we exclude self-interaction, so the results presented here are totally different from what we discussed in the previous subsection, as in the case of diffusive coupling case. It is very interesting to observe that the constraint (86) requires that the total excitatory and inhibitory

inputs to each neuron be balanced, a condition which is extensively discussed in the literature. We also note that the stability region for the synchronization state gets smaller with increasing delay τ.

Combining results presented in Section 2 and Fig. 14 and Fig. 15, we could easily assess the synchronization stability regions of a neuronal network with random interactions G_{ij}, regardless of whether it is a network with interactions of pulsed coupling or diffusive coupling. For example, from Fig. 14 and Eq. (31), we see that when

$$N < C \exp(\delta(-\langle G_{12} \rangle))$$

the synchronization state is stable, where $\delta(-\langle G_{12} \rangle)$ is the distance from $-\langle G_{12} \rangle$ to the boundary of 0-isoclines in Fig. 14 and G_{ij} is of Type I random variable.

In general, for a random matrix with i.i.d. standard normal distribution, Girko's circle law [62] tells us that all eigenvalues are uniformly distributed on the unit disk in the complex plane. To combine Girko's circle law with results presented here to obtain a sharper estimate of the stability regions would be interesting.

6 Conclusions

In the current paper, we presented a framework within which the stability of the synchronized solutions in networks with random interactions could be analyzed. For a given system the first important step is to establish the stability region. For some simple coupling functions this region can be found analytically. For more complex coupling functions this can only be done numerically. The second step is to establish constraints on the random coupling matrix to ensure the stability of the synchronized solutions. Such constraints can be exact in some simple cases. In more complex cases they are only approximate. This framework allowed us to extend Robert May's classic results on the stability of equilibrium solutions in randomly coupled linear systems to (a) randomly coupled nonlinear systems where the synchronized solution can be periodic or chaotic and (b) randomly coupled linear systems with transmission delays. In particular, we showed that a discrete time delay in the signal transmission defines a lower bound for the stability of the

synchronized solution; or in other words, any dispersion effects resulting in a distributed signal transmission with delay stabilize the synchronized solution relative to the case with no dispersion. Finally, we applied the framework to a network of neurons connected by diffusive or pulse delayed interactions. A systematic study was carried out to examine the synchronization properties of the network. The stability regions in this case can only be found numerically. In particular, for two HH neurons coupled diffusively, we found that there are three distinctive regions where different behaviors are observable. For two HH neurons with pulse coupling, it is found that excitatory coupling tends to synchronize more easily their activity. Not surprisingly, gap junction, rather than pulse coupling, have a wider parameter region where neuronal activity can be synchronized. A few general results on the stability of synchronized oscillations in networks of HH neurons were then presented. Based on the stability regions found numerically we considered the implications on the stability when random couplings are taken into account. This could help to pave the way for studying more general networks of neuronal models with random interactions such as the microcolumn networks [74, 75]

Theoretical studies such as the one we presented here have a number of limitations. For example, we have to require that each individual node in the network is identical in order to perform our analysis. This is obviously an oversimplification of many real world networks. Also, we do not expect the exact synchronization considered here to hold in the presence of noise.

Acknowledgment. J.F. was partially supported by grants from UK EPSRC(GR/R54569), (GR/S20574), and (GR/S30443). V.K.J. was supported by ONR N000140510104 and M.D. was supported by MH071620.

References

[1] L. Arnold, G. Papanicolaou, and V. Wihstutz, "Asymptotic analysis of the lyapunov exponent and rotation number of the random oscillator and applications," Siam J Appl Math. **46**, 427-450 (1986).

[2] R. Brown and N. F. Rulkov, "Designing a coupling that guarantees synchronization between identical chaotic systems," Phys. Rev. Lett. **78**, 4189 (1997).

[3] V.N. Belykh , I.V. Belykh, and M. Hasler, "Hierarchy and stability of partially synchronous oscillations of diffusively coupled dynamical systems," Phys. Rev. E **62**, 6332 (2000).

[4] V.N. Belykh , I.V. Belykh, and E. Mosekilde, "Cluster synchronization modes in an ensemble of coupled chaotic oscillators," Phys. Rev. E **63**, 036216 (2001).

[5] M. Barahona and L.M. Pecora, "Synchronization in small-world systems," Phys. Rev. Lett. **89**, 054101 (2002).

[6] N. Chatterjee and N. Gupte, "Synchronization in coupled sine circle maps," Phys. Rev. E **53**, 4457 (1996).

[7] H. Fujisaka and T. Yamada "Stability theory of synchronized motion in coupled-oscillator systems," Prog. Theor. Phys. **69**, 32 (1983).

[8] K. S. Fink , G. Johnson, T. L. Carroll, and L. M. Pecora , "Three coupled oscillators as a universal probe of synchronization stability in coupled oscillator arrays," Phys. Rev. E **61**, 5080 (2000).

[9] M. W. Hirsch and S. Smale , *Differential Equations, Dynamical Systems, and Linear Algebra* (Academy Press, New York, 1974).

[10] L. M. Pecora and T. L. Carroll, "Master stability functions for synchronized coupled systems," Phys. Rev. Lett. **80**, 2109 (1998).

[11] J. F. Heagy, L. M. Pecora, and T. L. Carroll, "Synchronous chaos in coupled oscillator-systems," Phys. Rev. E **50** 1874 (1994).

[12] S. Jankowski, A. Londei, C. Mazur, and A. Lozowski, "Synchronization and association in a large network of coupled Chua's circuits," Int. J Electronics **79**, 823 (1995).

[13] J. Jost and M. P. Joy, "Evolving networks with distance preferences," Phys. Rev. E **65**, 016201 (2002).

[14] L. Kocarev and U. Parlitz, "Generalized synchronization, predictability, and equivalence of unidirectionally coupled dynamical systems," Phys. Rev. Lett. **76**, 1816 (1996).

[15] R. Li and T. Erneux, "Stability conditions for coupled lasers-series coupling versus parallel coupling," Opt. Commun. **99**, 196 (1993).

[16] R. Li and T. Erneux, "Bifuracation to standing and traveling waves in large arrays of coupled lasers," Phys. Rev. A **49**, 1301 (1994).

[17] G. L. Oppo and R. Kapral, "Domain growth and nucleation in a discrete bistable system," Phys. Rev. A **36** 5820 (1987).

[18] K. Otsuka, R. Kawai, S. Hwong, J. Ko, and J. Chern, "Synchronization of mutually coupled self-mixing modulated lasers," Phys. Rev. Lett. **84**, 3049 (2000).

[19] J. G. Restrepo,E. Ott, and B. R. Hunt, "Desynchronization waves and localized instabilities in oscillator arrays," Phy. Rev. Lett. **93**, 114101 (2004).

[20] A. S. Pikovsky, "On the interaction of strange attractors," Phys Z. B **55**, 149 (1984).

[21] G. Paladin, M. Serva, "Analytic solution of the random Ising-model in one-dimension," Phys Rev Lett. **69**,706-709 (1992).

[22] R. May, "Will a large complex system be stable?" Science **238**, 413-414 (1972).

[23] T. A. Brody, J. Flores, J. B. French, P. A. Mello, A. Pandey, and S. S. M. Wong, "Random-matrix physics: spectrum and strength fluctuations," Review of Modern Physics **53**, 385-479 (1981).

[24] M. Isopi and C. M. Newman, "The triangle law for Lyapunov exponents of large random matrices," Commun. Math. Phys. **143**, 591-598 (1992).

[25] G. H. Golub and C. F. Van Loan, *Matrix Computations*, (Johns Hopkins University Press, Baltimore, 1996).

[26] V. K. Jirsa and M. Z. Ding, "Will a large complex system with time delays be stable?" Phys Rev Lett. **93**, 070602 (2004).

[27] C. Y. Lee and D. b. Williams, "Generalized iterative methods for enhancing contaminated chaotic Signals," IEEE T CIRCUITS-I **44** 501-512 (1997).

[28] R. Roy and K. S. Thornburg, "Experimental synchronization of chaotic lasers," Phys. Rev. Lett. **72** 2009 (1994).

[29] N. F. Rulkov and M. M. Sushchik, "Robustness of synchronized chaotic oscillations," Int. J. Bifurcation and Chaos **7**, 625 (1997).

[30] W. Feller, *An Introduction to Probability Theory and Its Applications*, (John Wiley & Son, New York, 1971).

[31] E. L. Berlow, A. M. Neutel, and J. E. Cohen et al. "Interaction strengths in food webs: issues and opportunities," J. ANIM. ECOL. **73** 585-598 (2004).

[32] J. E. Cohen and C. M. Newman, "The stability of large random matrices and their products," The Annals of Probability **12**, 283-310 (1984).

[33] J. E. Cohen and C. M. Newman, "When will a large complex system be stable?" J. Theor. Biol. **113**, 153-156 (1985).

[34] J. E. Cohen and C. M. Newman, "Dynamic basis of food web organzanition," Ecology **69**, 1655-1664 (1988).

[35] J. E. Cohen and T. Lucak, and C. M. Newman et al. "Stochastic structure and nonlinear dynamics of food webs-qualitative stability in a lotka volterra cascade model," P. Roy. Soc. Lond. B Bio. **240**,607-627 (1990).

[36] J. E. Cohen and C. M. Newman, "Host-parasite relations and random zero-sum games-the stabilizing effect of strategy diversification," Am Nat. **133**,533-552 (1989).

[37] X. Chen and J. E. Cohen, "Transient dynamics and food-web complexity in the Lotka-Volterra cascade model," P Roy. Soc. lond. B Bio. **268** 869-877 (2001).

[38] S. Gemam, "The spectral-radius of large random matrices," Ann. Probab. **14**, 1318-1328 (1986).

[39] P. M. Gade, "Synchronization of oscillators with random nonlocal connectivity," Phys Rev E. **54** 64-70 (1996).

[40] T. Hogg, B. A. Huberman, and J. M. Mcglade , "The stability of ecosystems," P Roy. Soc. Lond. B Bio. **237** 43-51 (1989).

[41] E. Key, "Computable examples of the maximal Lyapunov exponent," Probab. Theory Rel. **75**, 97-107 (1987).

[42] C. W. Li, and G.L. Blankenship, "Almost sure stability of linear stochastic-systems with poisson-process coefficients," Siam J. Appl. Math. **46**, 875-911 (1986).

[43] R. Lima, and M. Rahibe, "Exact Lyapunov exponent for infinite products of random matrices," J. Phys. A-Math. **27**, 3427-3437 (1994).

[44] C. M. Newman, "The distribution of Lyapunov exponents exact results for random matrices," Commun. Math. Phys. **103** 121-126 (1986).

[45] J. F. Feng, M. Shcherbina, and B. Tirozzi, "Dynamics of large complex dynamics," submitted.

[46] Y. C. Deng, M. Z. Ding, J. F. Feng, "Synchronization in stochastic coupled systems: theoretical results," J. Phys. A **37** 2163-2173 (2004).

[47] G. Hu, J. Yang, and W. Liu, "Instability and controllability of linearly coupled oscillators: Eigenvalue analysis," Phys. Rev. E **58** 4440 (1998).

[48] H. M. Hastings, F. Juhasz, M. A. Schreiber, "Stability of structured random matrices," P Roy. Soc. Lond. B Bio. **249**,223-225 (1992).

[49] Y. Chen, R. Rangarajan, and M. Ding, "General Stability Analysis of Synchronized Dynamics in Coupled Systems," Phys. Rev. E **67**, 026209 (2003).

[50] Y. Peres, "Domains of analytic continutation for top lyapunov exponent," Ann. I H Poincare-pr. **28** 131-148 (1992).

[51] We note that, since the Lyapunov exponent h_{max} is computed from typical initial conditions, the stability here is with respect to the blowout bifurcation. Bubbling transition can occur while the parameters are still within the bound derived in this work. For details on these phenomena see E. Ott and J. C. Sommerer, "Blowout bifurcations-The occurrence of riddled basins and

on off intermittency" Phys. Lett. A. **188**, 39 (1994); P. Ashwin , J. Buescu and I. Stewart, "Bubbling of attractors and synchronization of chaotic oscillators," Phys. Lett. **193**, 126 (1994); S. C. Venkataramani et al, "Transitions to bubbling of chaotic systems," Phys. Rev. Lett. **77**, 5361 (1996); and S. C. Venkataramani et al, "Bubbling transition," Phys. Rev. E **54**, 1346 (1996).

[52] J. P. Eckmann, and C. E. Wayne, "The largest Lyapunov exponent for random matrices and directed polymers in a random environment," Commun. Math. Phys. **121**,147-175 (1989).

[53] R. A. Horn and C. R. Johnson, *Matrix Analysis* (Cambridge University Press, Cambridge, 1985).

[54] M. R. Leadbetter, Georg Lindgren, and Holger Rootzén, *Extremes and Related Properties of Random Sequences and Processes*, (Springer-Verlag, New York, 1983).

[55] G. Rangarajan and M. Ding, "Stability of synchronized chaos in coupled dynamical systems," Phys. Lett. A **296** 204 (2002).

[56] D. J. Gauthier and J. C. Bienfang, "Intermittent loss of synchronization in coupled chaotic oscillators: Toward a new criterion for high-quality synchronization," Phys. Rev. Lett. **77**,1751 (1996).

[57] K. L. Cooke, Z. Grossman, "Discrete delay, distributed delay and stability switches," J. Math. Analysis and Appl. **86**, 592 (1982).

[58] R. Datko, "Procedure for determination of exponential stability of certain differential-difference equations," Quart. Appl. Mathematics. **36**,279 (1978).

[59] L. Chen, K. Aihara, "Stability of Genetic Regulatory Networks with Time Delay," IEEE Transactions Circ. Systems **49**, 5, 602-608 (2002).

[60] J. Feng , D. Brown, and G. Li, "Synchronization due to common pulsed input in Stein's model," Phys. Rev. E **61**, 2987-2995 (2000).

[61] J. F. Feng , *Computational Neuroscience: A Comprehensive Approach*, (Chapman and Hall/CRC Press, Boca Raton, 2003).

[62] Girko V.L. (1990) *Theory of Random Determinants*, Boston, MA: Kluwer.

[63] D. Hansel and H. Sompolinsky, "Synchronization and computation in a chaotic neural network," Phys. Rev. Lett. **68**,718 (1992).

[64] D. Hansel, "Int. J Synchronized chaos in local cortical circuits," Neural Sys. **7**, 403 (1996).

[65] D. Brown, J. F. Feng, and S. Feerick, "Variability of firing of Hodgkin-Huxley and FitzHugh-Nagumo neurons with stochastic synaptic input," Phys. Rev. Lett. **82**, 473 (1999).

[66] A. Hodgkin and A. Huxley, "A Quantitative Description of Membrane Current and its Application to Conduction and Excitation in Nerve," J. Physiol. **117**, 500 (1952).

[67] A. Crisanti, G. Paladin, A.Vulpiani, "Generalized Lyapunov exponents in high-dimensional chaotic dynamics and products of large random matrices," J. Stat. Phys. **53**, 583-601 (1998).

[68] T. Bem and J. Rinzel, "Short duty cycle destabilizes a half-center oscillator, but gap junctions can restabilize the anti-phase pattern," J. Neurophysiol. **91**, 693 (2004).

[69] J. P. Eckmann and D. Ruelle, "Ergodic-theory of chaos and strange attractors," Rev. Mod. Phys. **57**, 617 (1985).

[70] M. Dhamala, V. K. Jirsa, and M. Ding, "Enhancement of neural synchrony by time delay," Phys. Rev. Lett. **92** 074104 (2004).

[71] I. S. Labouriau and H. M. Rodrigues, "Synchronization of coupled equations of Hodgkin-Huxley type," Dynam. Cont. Dis. Ser. A. **10**, 463 (2003).

[72] P. C. Bressloff, "Mean-field theory of globally coupled integrate-and-fire neural oscillators with dynamic synapses," Phys. Rev. E **60**, 2160 (1999).

[73] F. Pasemann, "Synchronized chaos and other coherent states for two coupled neurons," Physica D **128**, 236 (1999).

[74] W. Maass, T. Natschläger, and H. Markram , in *Computational Neuroscience: A Comprehensive Approach*, edited by J. F. Feng (Chapman and Hall/CRC Press, Boca Raton, 2003), Chap. 18.

[75] A. Destexhe and E. Marder, "Plasticity in single neuron and circuit computations," *Nature* **431**, 789 (2004).

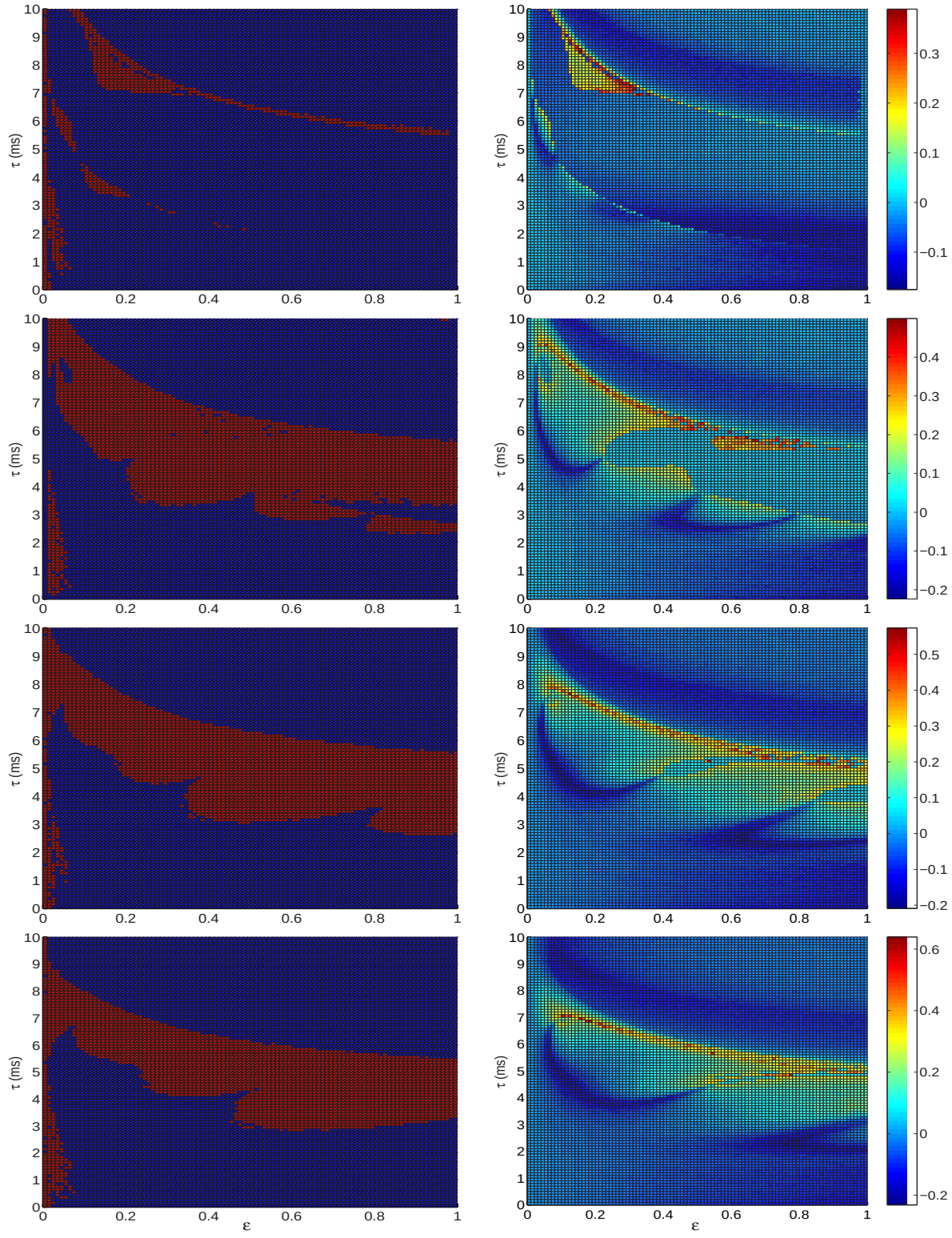

Figure 9: (Color online) Stability of synchronized oscillations for a system of two HH neurons with diffusive coupling. (**Right**) Color intensity represents the maximum transverse Lyapunov exponent, $\lambda_\perp$, in the $(\tau - \epsilon)$ space. **(Left)** Similar to the right figures, but it represents the region of stability (blue) and unstable regions (red) in the $(\tau - \epsilon)$ space. Results were obtained for $I_{ext} = 7, 10, 15, 20$ μA/cm^2 (from top to bottom).

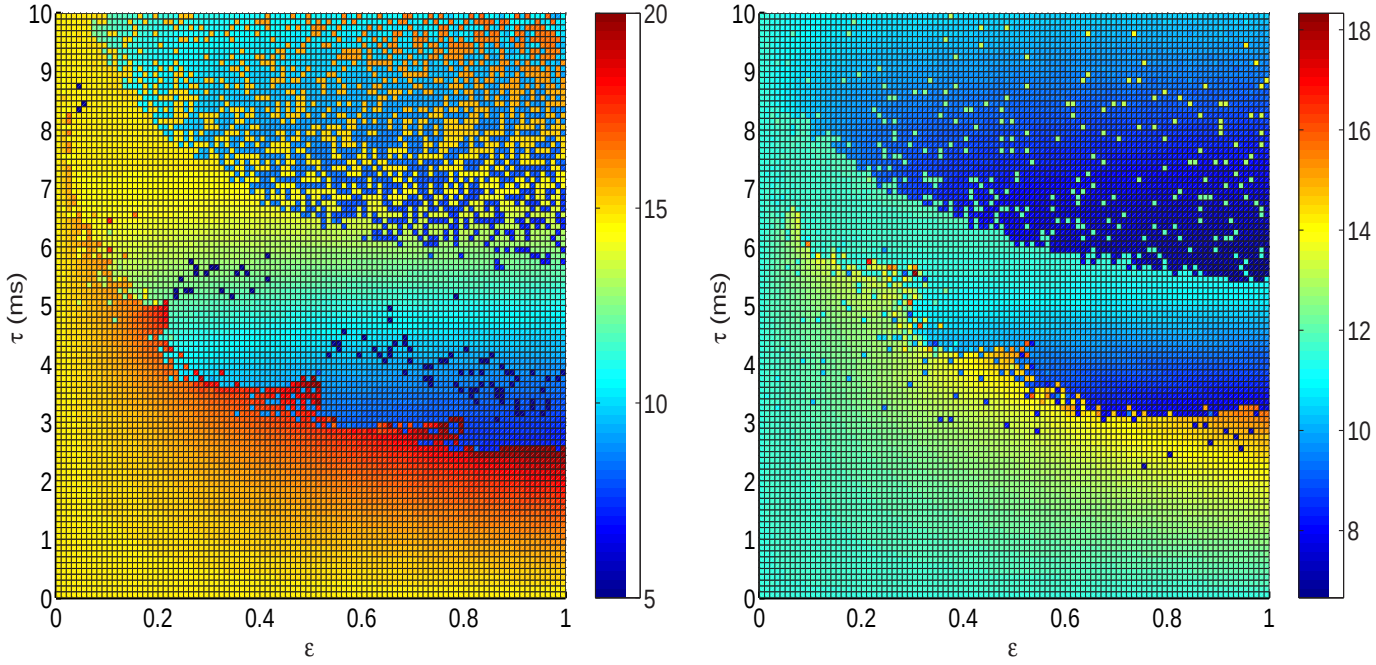

Figure 10: (Color online) The period T of the oscillations as observed in a system of two diffusively coupled HH neurons. Results were obtained for $I_{ext} = 10$ μA/cm^2 (left), and $I_{ext} = 20$ μA/cm^2 (right). For fixed parameters, the initial state is chosen randomly and quenched state (middle region) is represented by a 'hole' in the figure, comparing with Fig. 9.

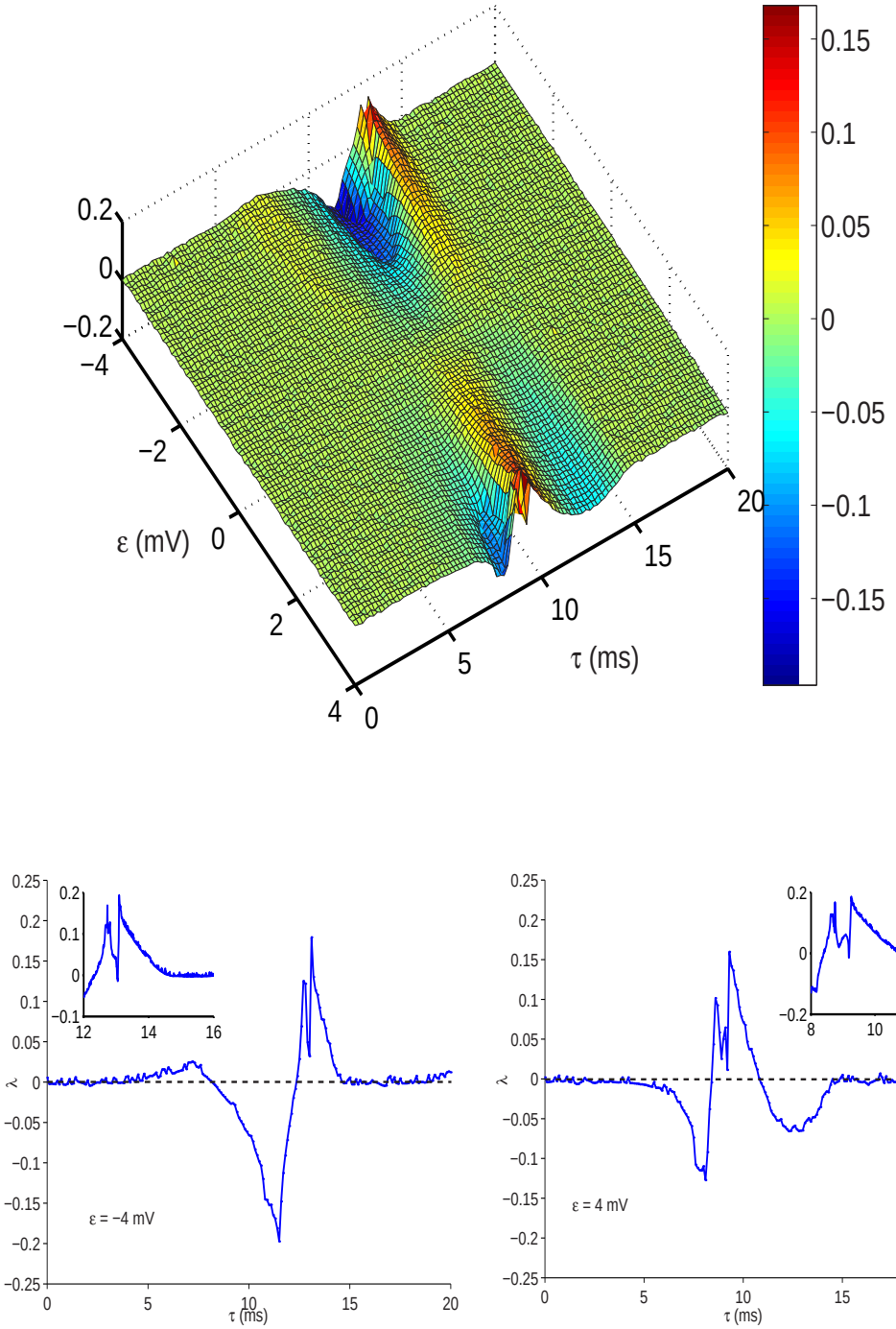

Figure 11: (Color online) Upper panel: Stability of synchronized oscillations for a system of two HH neurons with pulse coupling. Color intensity represents the maximum transverse Lyapunov exponent, $\lambda_\perp$, in the $(\tau - \epsilon)$ space. Results were obtained for $I_{ext} = 10$ μA/cm^2. Bottom left: The maximum transverse Lyapunov exponent, $\lambda_\perp$, as a function of time delay for $\epsilon = -4$ mV. The inset shows a blow-up around the maximum. Bottom right: The maximum transverse Lyapunov exponent, $\lambda_\perp$, as a function of time delay for $\epsilon = 4$ mV. The inset shows a blow-up around the maximum.

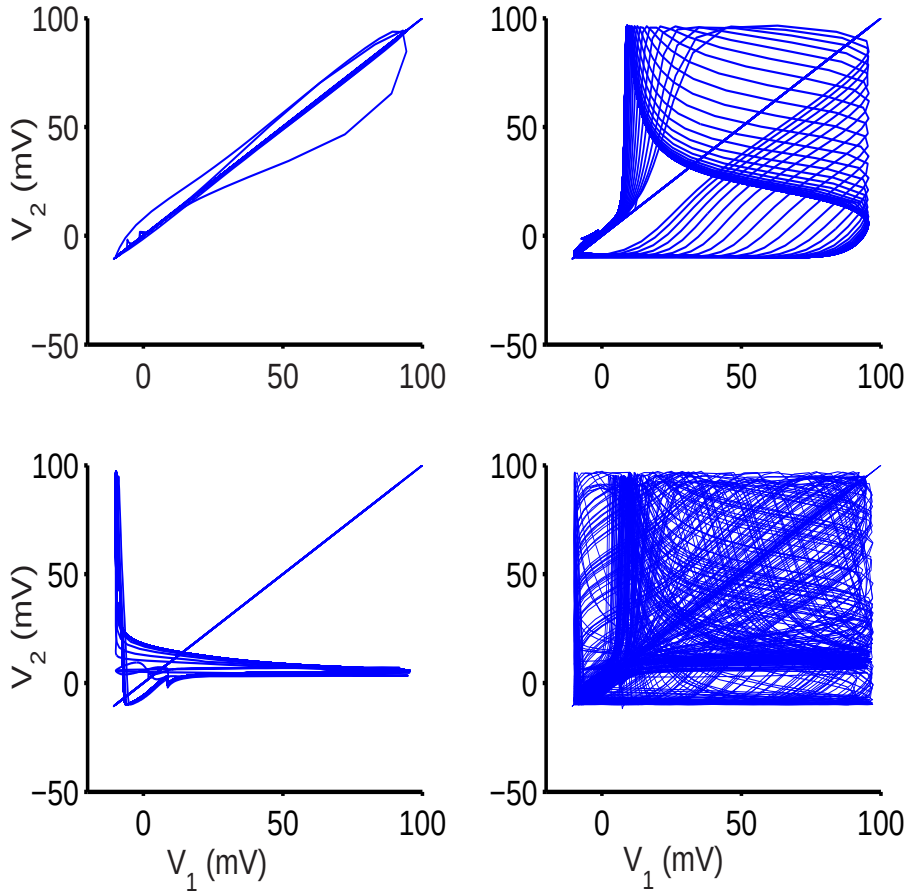

Figure 12: Examples of trajectories in the V_1-V_2 plan which correspond to different dynamical behaviors: synchronization (**top left**; $\epsilon = 3$ mV, $\tau = 8$ ms); anti-phase locking (**bottom left**, $\epsilon = 4$ mV, $\tau = 13$ ms); phase-locking (**top right**, $\epsilon = -2$ mV, $\tau = 8$ ms) and chaos (**bottom right** $\epsilon = -4$ mV, $\tau = 11.6$ ms, . The system is initialized on the synchronous manifold, and let evolve freely until an instantaneous perturbation is applied which disrupts the symmetry of the solution. The trajectories in the V_1-V_2 reveal different kinds of attractors, which are manifest when the synchronous manifold is destabilized. For positive coupling (upper panels), once displaced out of the synchronous manifold, the system gets attracted to a phase-locked oscillatory state; for negative coupling (lower panels), the system shows aperiodic oscillations which are indicative of a seemingly chaotic (strange) attractor.

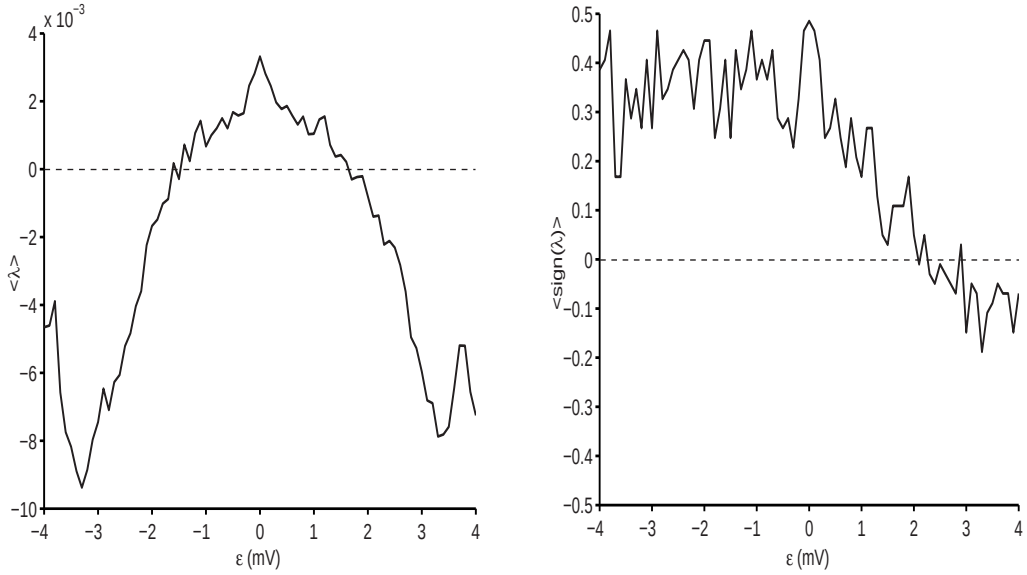

Figure 13: (Left) Average of $\lambda_\perp$ over $\tau \in [0, 20]$ msec; (right) average of sign($\lambda_\perp$) over $\tau \in [0, 20]$msec.

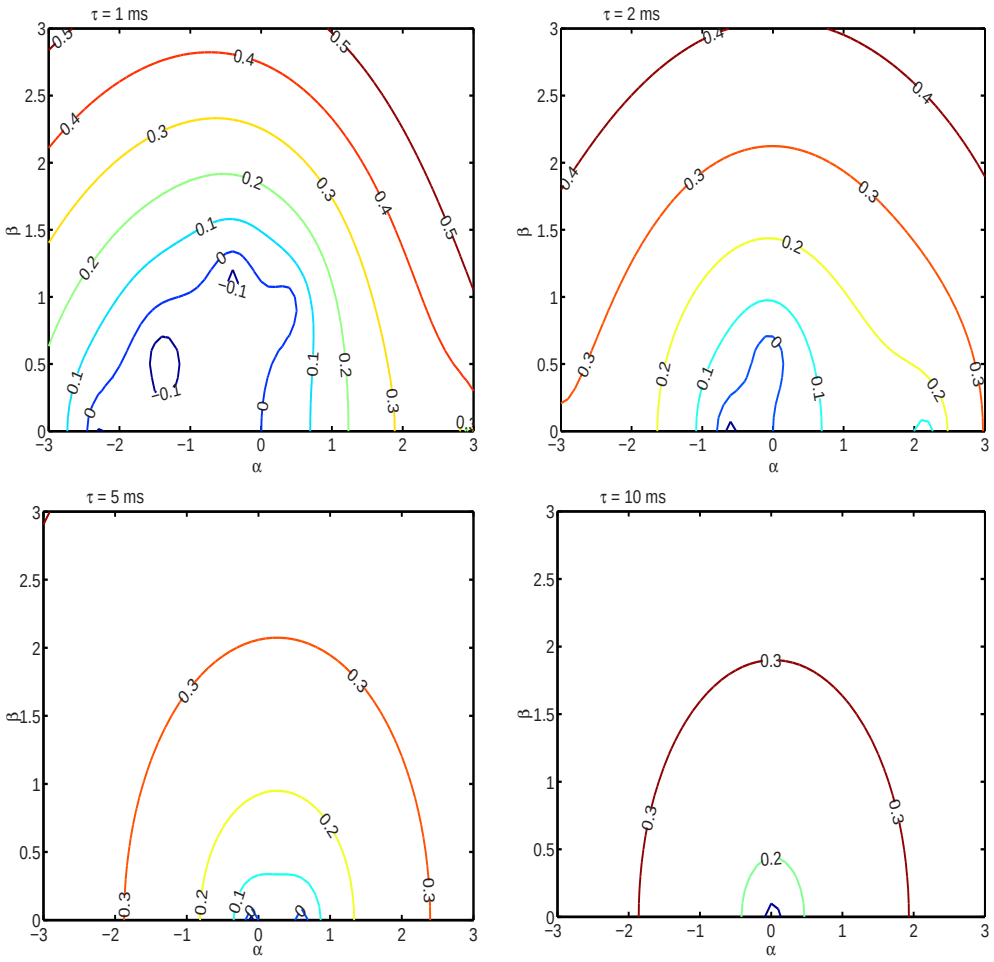

Figure 14: (Color online) Upper Panel: Master stability function at $\tau = 1$ ms (top) and $\tau = 2$ ms (right), for a system of diffusively coupled HH neurons. The lines are isoclines for the constant maximum Lyapunov exponent. Bottom Panel: Master stability function at $\tau = 5$ ms (top) and $\tau = 10$ ms (bottom), for a system of diffusively coupled HH neurons. The lines are isoclines for the constant maximum Lyapunov exponent.

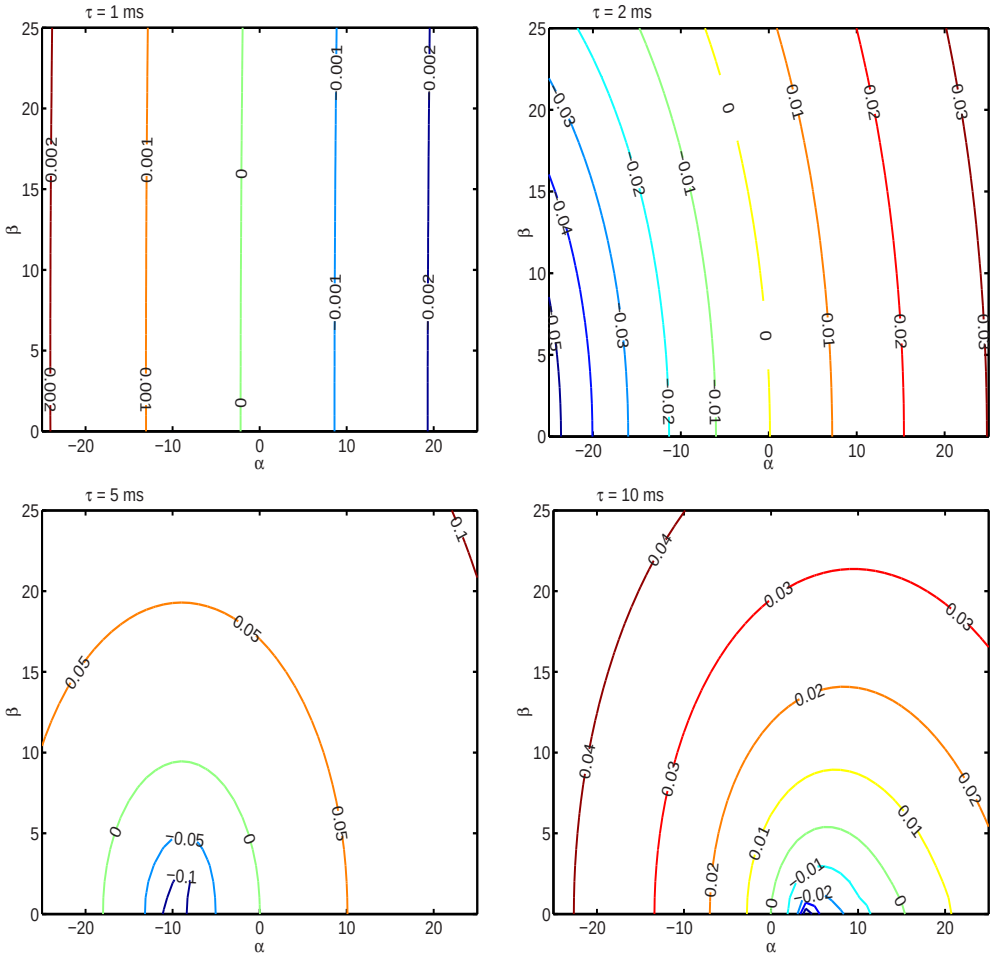

Figure 15: (Color online) Master stability function at $\tau = 1$ ms (top left), $\tau = 2$ ms (top right), $\tau = 5$ ms (bottom left), and $\tau = 10$ ms (bottom right), for a system of pulse coupled HH neurons. The lines are isoclines for the constant maximum Lyapunov exponent.